

Carbonate stromatolites from a Messinian hypersaline setting in the Caltanissetta Basin, Sicily: petrographic evidence of microbial activity and related stable isotope and rare earth element signatures

ELVIRA OLIVERI*, RODOLFO NERI*, ADRIANA BELLANCA* and ROBERT RIDING†

*Dipartimento di Chimica e Fisica della Terra (CFTA), Università di Palermo, Via Archirafi 36, 90123 Palermo, Italy (E-mail: neri@unipa.it)

†Department of Earth and Planetary Sciences, University of Tennessee, Knoxville, TN 37996, USA

Associate Editor: Tracy Frank

ABSTRACT

Lower Messinian stromatolites of the Calcare di Base Formation at Sutera in Sicily record periods of low sea-level, strong evaporation and elevated salinity, thought to be associated with the onset of the Messinian Salinity Crisis. Overlying aragonitic limestones were precipitated in normal to slightly evaporative conditions, occasionally influenced by an influx of meteoric water. Evidence of bacterial involvement in carbonate formation is recorded in three dolomite-rich stromatolite beds in the lower portion of the section that contain low domes with irregular crinkly millimetre-scale lamination and small fenestrae. The dominant microfabrics are: (i) peloidal and clotted dolomicrite with calcite-filled fenestrae; (ii) dolomicrite with bacterium-like filaments and pores partially filled by calcite or black amorphous matter; and (iii) micrite in which fenestrae alternate with dark thin wispy micrite. The filaments resemble *Beggiatoa*-like sulphur bacteria. Under scanning electron microscopy, the filaments consist of spherical aggregates of dolomite, interpreted to result from calcification of bacterial microcolonies. The dolomite crystals are commonly arranged as rounded grains that appear to be incorporated or absorbed into developing crystal faces. Biofilm-like remains occur in voids between the filaments. The dolomite consistently shows negative $\delta^{13}\text{C}$ values (down to -11.3‰) and very positive $\delta^{18}\text{O}$ (mean value 7.9‰) that suggest formation as primary precipitate with a substantial contribution of organic CO_2 . Very negative $\delta^{13}\text{C}$ values (down to -31.6‰) of early diagenetic calcite associated with the dolomite suggest contribution of CO_2 originating by anaerobic methane oxidation. The shale-normalized rare earth element patterns of Sutera stromatolites show features similar to those in present-day microbial mats with enrichment in light rare earth elements, and M-type tetrad effects (enrichment around Pr coupled to a decline around Nd and a peak around Sm and Eu). Taken together, the petrography and geochemistry of the Sutera stromatolites provide diverse and compelling evidence for microbial influence on carbonate precipitation.

Keywords Calcare di Base, Messinian, microbial carbonate, petrography, rare earth elements, Sicily, stable isotopes, stromatolites.

INTRODUCTION

Microbes can play important roles in the production, accumulation and diagenesis of sediments (Nealson, 1997; Riding & Awramik, 2000; Tucker, 2001; and references therein), even though their action and impact may differ greatly according to the types of sediments and environments. Castanier *et al.* (2000) emphasized the relationship between carbonate precipitation and organic matter enrichment in heterotrophic bacterial communities. These microbes can orchestrate CaCO_3 precipitation and stromatolite formation, lithifying organosedimentary structures that show a layered structure (Riding, 2000; Dupraz & Visscher, 2005). In particular, sulphate-reducing bacteria (SRB) have been suggested to mediate anaerobic carbonate precipitation in microbial mats (Jørgensen & Cohen, 1977; Lyons *et al.*, 1984; Canfield & Des Marais, 1991; Visscher *et al.*, 1998, 2000; Reid *et al.*, 2000; Sprachta *et al.*, 2001; Dupraz *et al.*, 2004). Many researchers have highlighted the role that SRB can play in primary dolomite formation (Compton, 1988; Middleburg *et al.*, 1990; Vasconcelos *et al.*, 1995; Vasconcelos & McKenzie, 1997; Wright, 1999; Van Lith *et al.*, 2003; Wright & Wacey, 2005; Meister *et al.*, 2007). Carbon isotopic values can indicate bacterial involvement in carbonate precipitation (Murata *et al.*, 1969; Claypool & Kaplan, 1974; Compton, 1988). The distribution of geochemical elements, particularly rare earth elements (REE) that are essentially immobile during diagenesis, can also provide useful information to identify bacterial contributions in sedimentary deposits (Takahashi *et al.*, 2005).

In the Italy area, during the Messinian Salinity Crisis (MSC), the transition from marine to evaporitic conditions may be reflected in a variety of different sedimentary deposits (Tripoli, Calcare di Base and Gessoso-Solfifera Formations), which contain a record of marked environmental changes. An example of this is the Calcare di Base Formation of Southern Italy, the significance of which is still debated (Rouchy & Caruso, 2006; Guido *et al.*, 2007; Roveri *et al.*, 2008). On the basis of very negative carbon isotope signatures, McKenzie *et al.* (1979–1980) and Bellanca *et al.* (1983, 1986) ascribed precipitation of early diagenetic carbonate, in diatomites of the Messinian Tripoli Formation in Sicily, to the action of SRB; however, at that time, no petrographic evidence of bacterial biomineralization was provided.

This study centres on dolomite-rich stromatolites from the Calcare di Base Formation in the Caltanissetta Basin, near Sutera town, Sicily (Fig. 1). The focus was: (i) investigation of the processes promoting carbonate precipitation in these stromatolite beds that formed in a Messinian hypersaline setting; and (ii) relating the petrographic evidence of microbial activity to geochemical (O and C isotopes, Sr, REE) signatures. Rare earth element patterns are used here for the first time to highlight and discuss the imprint of bacterial activity in stromatolites from the Calcare di Base.

GEOLOGICAL SETTING

During the Miocene, the Mediterranean region was affected by the MSC (Hsü *et al.*, 1973). This important evaporitic event resulted from isolation of the Mediterranean Sea from the world ocean. Large volumes of Messinian evaporites were deposited in a series of sub-basins, delimited by local barriers, within a large pre-Messinian basin (Cavazza & Wezel, 2003). Evaporite deposition was preceded in many Mediterranean peripheral basins by formation of cyclic, thinly bedded diatom-rich deposits (e.g. the Tripoli Formation in Sicily) (Rouchy, 1982; Bellanca *et al.*, 1986; Martín & Braga, 1994; Clauzon *et al.*, 1996; Riding *et al.*, 1998, 2000). A similar sequence was deposited in some deep-sea areas (Ocean Drilling Program (ODP) Site 372, Cita *et al.*, 1978; ODP Site 654, Pierre & Rouchy, 1990). The increase in biosiliceous productivity has been linked to a variety of factors, e.g. upwelling of marine deep waters (McKenzie *et al.*, 1979–1980; Rouchy, 1986; Müller & Hsü, 1987) and increase in terrestrial nutrient supply (Van der Zwaan, 1979; Hodell *et al.*, 1994; Rouchy *et al.*, 1998), related to either increasing isolation of the Mediterranean (McKenzie *et al.*, 1979–1980) or global eustatic control (Suc *et al.*, 1995), or to both of these (Rouchy, 1982; Rouchy & Saint-Martin, 1992).

The onset of MSC evaporite deposition has been suggested to have been synchronous over the entire Mediterranean Basin and to have occurred between 5.70 to 5.96 Ma (Gautier *et al.*, 1994; Krijgsman *et al.*, 1999, p. 654; Cavazza & Wezel, 2003). In contrast, on the basis of magnetostratigraphic and sequence-stratigraphic data from evaporitic deposits in Sicily, Butler *et al.* (1995, 1999) suggested that evaporite onset was diachronous, over a period of at least 800 ka, in

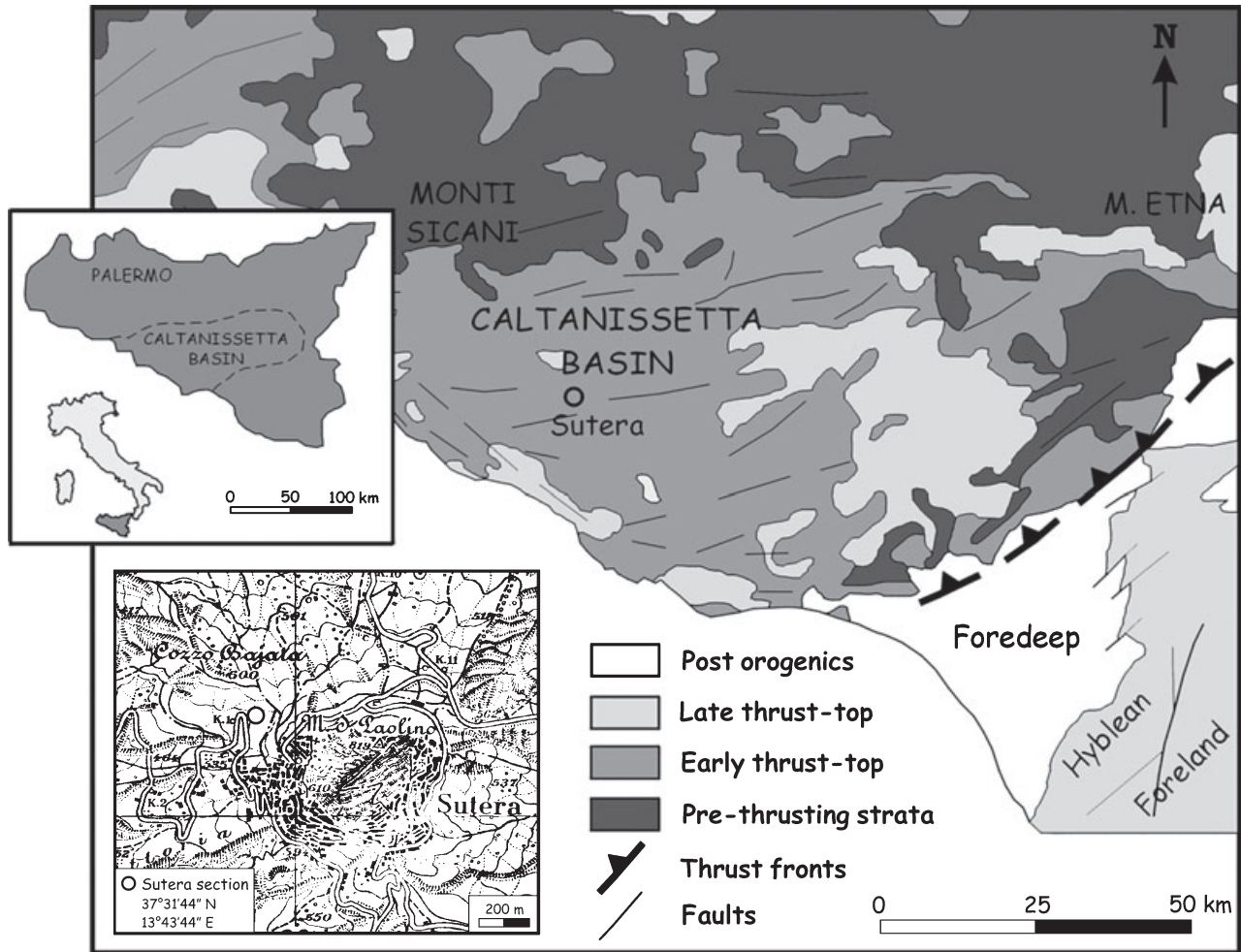


Fig. 1. General geological setting of the Caltanissetta Basin, Sicily (simplified from Butler *et al.*, 1995) showing the location of the Sutera section.

the different sub-basins of the Caltanissetta Basin. Riding *et al.* (1998) also proposed that in shallow marginal Mediterranean basins evaporite deposition tended to either pre-date or post-date the evaporites of the deeper Mediterranean and that these marginal evaporites are not completely contemporaneous with those of the deeper basins.

The Caltanissetta Basin (Fig. 1) contains one of the best exposed records of Messinian strata (Krijgsman & Zachariasse, 1994; Hilgen *et al.*, 1995), deposited within a series of thrust-related synclines (Butler *et al.*, 1995); these form the outer part of the Maghrebain Chain in a zone between the Northern Sicilian Mountains (European plate) and the Hyblean Plateau (African foreland). In this area, the classic stratigraphic model recognizes two main evaporitic units separated by an intra-Messinian tectonic unconformity (Decima & Wezel, 1971; Butler *et al.*, 1995; Rouchy & Caruso, 2006). From bottom to top, the lower unit consists of the Tripoli Formation,

Calcare di Base Formation (evaporitic limestone), Lower Gypsum and Salt. According to the classic view, the Calcare di Base was deposited in the shallow portion of the Caltanissetta Basin and represents the stratigraphic equivalent of the Lower Gypsum that occurs in the deepest portion of the basin. The upper unit is formed by the Upper Gypsum overlain by the Arenazzolo Formation, siliciclastic lacustrine and fluvial/alluvial facies (Decima & Wezel, 1973; Cita & Colombo, 1979), in turn capped by the pelagic Early Pliocene Trubi Formation, which marks the re-establishment of normal marine conditions as a consequence of flooding from the Atlantic (Cita, 1975; Di Stefano *et al.*, 1999; Rouchy *et al.*, 2001).

According to Roveri *et al.* (2001) and Manzi *et al.* (2007), in Sicily as well as in the Northern Apennines, the Lower Gypsum includes both primary gypsum (shallow water facies) and resedimented gypsum (deep water facies). In Sicily, the primary Lower Gypsum was deposited only in the

innermost wedge-top basins and in the Hyblean foreland ramp basins, and is not associated with the Salt and/or the Calcare di Base (Roveri *et al.*, 2008).

In many outcrops, the Calcare di Base Formation consists of massive pale cream limestone, commonly brecciated and intercalated with dolostones, grey clays and marls (Ogniben, 1957, 1963; Decima & Wezel, 1973; Decima *et al.*, 1988). At Sutera, the lower portion of the stratigraphic sequence includes three stromatolite beds. The lowest of these is in stratigraphic contact with marls of the underlying Tripoli Formation. The Calcare di Base is commonly characterized by the presence of halite moulds, calcite pseudomorphs after gypsum, and peloidal microfabrics that have been linked to bacterial activity (Tamajo, 1961; Ogniben, 1963; Decima *et al.*, 1988). It also contains sulphur-bearing limestone derived from bacterial sulphate reduction (BSR).

For many authors, the Calcare di Base is laterally equivalent to the Lower Gypsum and marks the onset of the MSC, preceding deposition of the sulphate and salt evaporites of the Gessoso-Solfifera Formation (McKenzie, 1985; Bellanca & Neri, 1986; Decima *et al.*, 1988; Caruso *et al.*, 1997; Bellanca *et al.*, 2001; Rouchy & Caruso, 2006). In contrast, taking the view that the Calcare di Base is mostly a non *in situ* brecciated limestone, Roveri *et al.* (2008) argue that its base represents a regional-scale unconformity and that it does not mark the onset of the MSC. Roveri *et al.* (2008) support Hilgen & Krijgsman (1999) in recognizing the dolostones above the Tripoli Formation as the only part of the Calcare di Base that is the lateral equivalent of the primary Lower Gypsum.

Sutera stratigraphy

The section studied here is within the Caltanissetta Basin (13°43'44" E, 37°31'44" N) and is located about 2 km north-west of Sutera town (Fig. 1). At Sutera, the Calcare di Base overlies the Lower Messinian Tripoli Formation which, in turn, overlies Tortonian clays of the Terravecchia Formation. The sequence studied comprises the uppermost 3 m of the Tripoli Formation and the lower *ca* 16 m of the Calcare di Base Formation (Fig. 2A). The passage between these two formations is marked by the three dolomite-rich stromatolite beds that are the focus of this study (Fig. 2B to E). These beds display millimetre-scale stratiform layering (flat stromatolites)

(Fig. 2E) and alternate with dolomitic marls (of variable thickness), laminated dolostones (up to 1 m thick) and millimetre-thick claystone beds (Fig. 2A). Higher in the section, claystone beds up to 5 m thick alternate with aragonitic limestones up to 4 m thick.

Stromatolites

The lowest stromatolitic bed (I in Fig. 2A) is 37 cm thick, grey to brown in colour, and exhibits very low domes, irregular laminae (1.5 to 3 mm), and intense bioturbation (Fig. 3A). The middle stromatolitic bed (II in Fig. 2A) is 44 cm thick and consists of very thin alternating brown and grey laminae, with fine open pores and domes up to 4.5 cm wide and 1.5 cm high (Fig. 3B). Higher in the same bed, the alternation of laminae is interrupted by grey to dark-grey crinkly layers (Fig. 3C). The uppermost stromatolitic bed is 62 cm thick (III in Fig. 2A) with thick to thin layers (1 to 5.5 mm), very low domes, small fenestral pores and vertical burrows (Fig. 3D).

ANALYTICAL METHODS

A total of 72 samples was collected from the Sutera section. In the laboratory, sub-samples were obtained from the stromatolite layers. Each sample was crushed in an agate mortar to obtain fine uncontaminated powders.

Bulk sample mineralogy was determined by powder X-ray diffraction using a Philips PW14 1373 (Koninklijke Philips Electronics NV, Amsterdam, The Netherlands) with Cu-K α radiation filtered by a monochromator crystal and a scanning speed of 2°2 θ /min. The relative proportions of minerals were determined using the methods and data of Schultz (1964) and Barahona *et al.* (1982). Petrographic thin sections of selected carbonate samples were observed using polarized light microscopy. Scanning electron microscope (SEM) investigations were performed on fresh broken surfaces and on polished, carbon-coated thin sections, using a LEO 440 with EDS system OXFORD ISIS 300 Link and a Si (Li) PENTAFET detector (Leo Electron Microscopy Ltd., Cambridge, UK).

Carbonate oxygen and carbon isotopic compositions were obtained from bulk-rock samples. To remove organic matter, samples were roasted for 40 min at 370 °C in high-vacuum glass tubes, then dissolved in 100% phosphoric acid at 25 °C under high vacuum for 12 h for calcite and

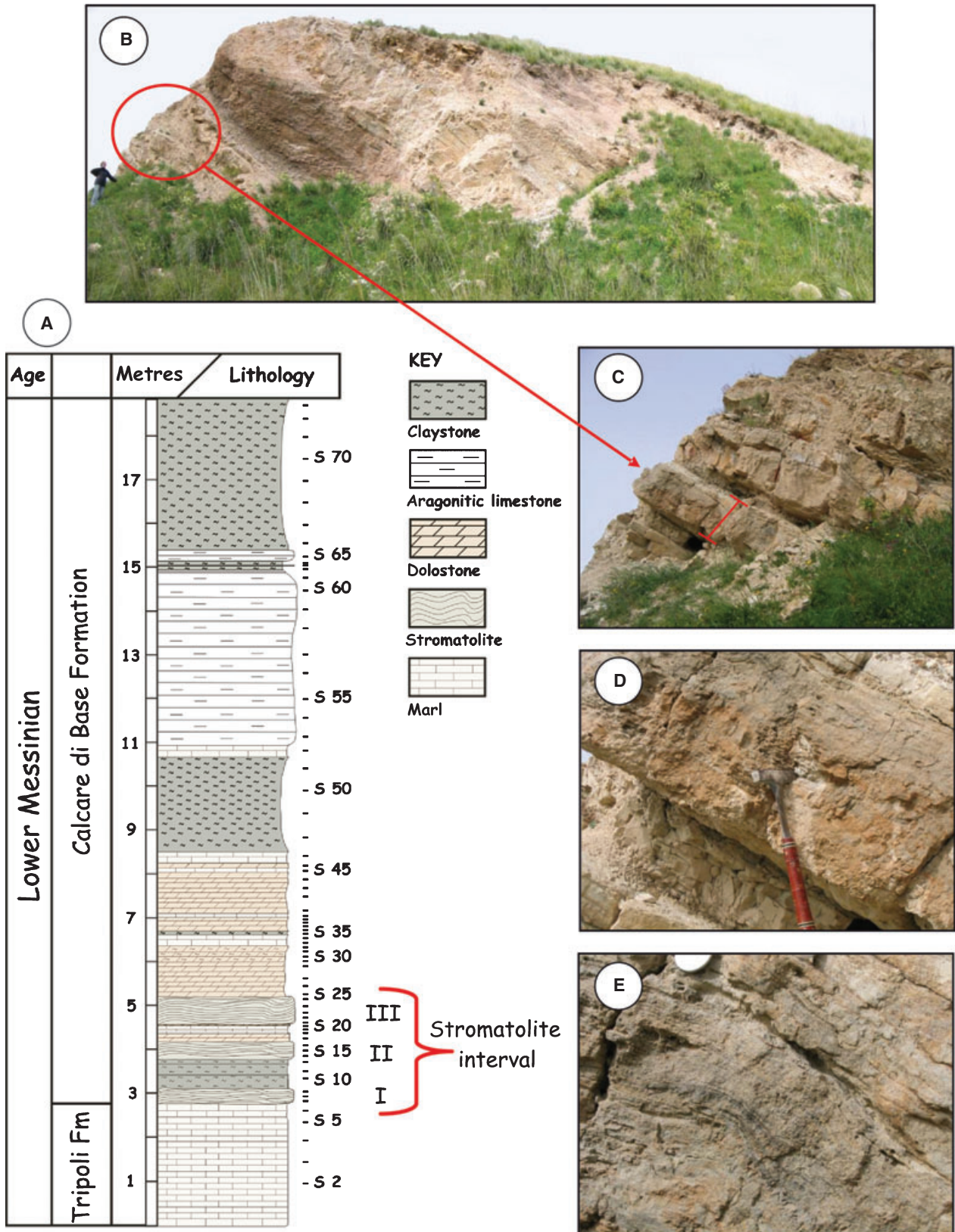


Fig. 2. Sutera section. (A) Lithological column showing sample horizons (S 2 to S 73) and the three stromatolite beds (I, II and III). (B) to (E) Progressively closer views of the stratigraphic succession and stromatolite beds. Person for scale in (B) is ca 1.8 m tall. In (C) the red arrow points to the stromatolite unit which is also shown by the red bar. Scale size on (C) = 44 cm; hammer size on (D) = 31.5 cm; coin size on (E) = 2.5 cm.

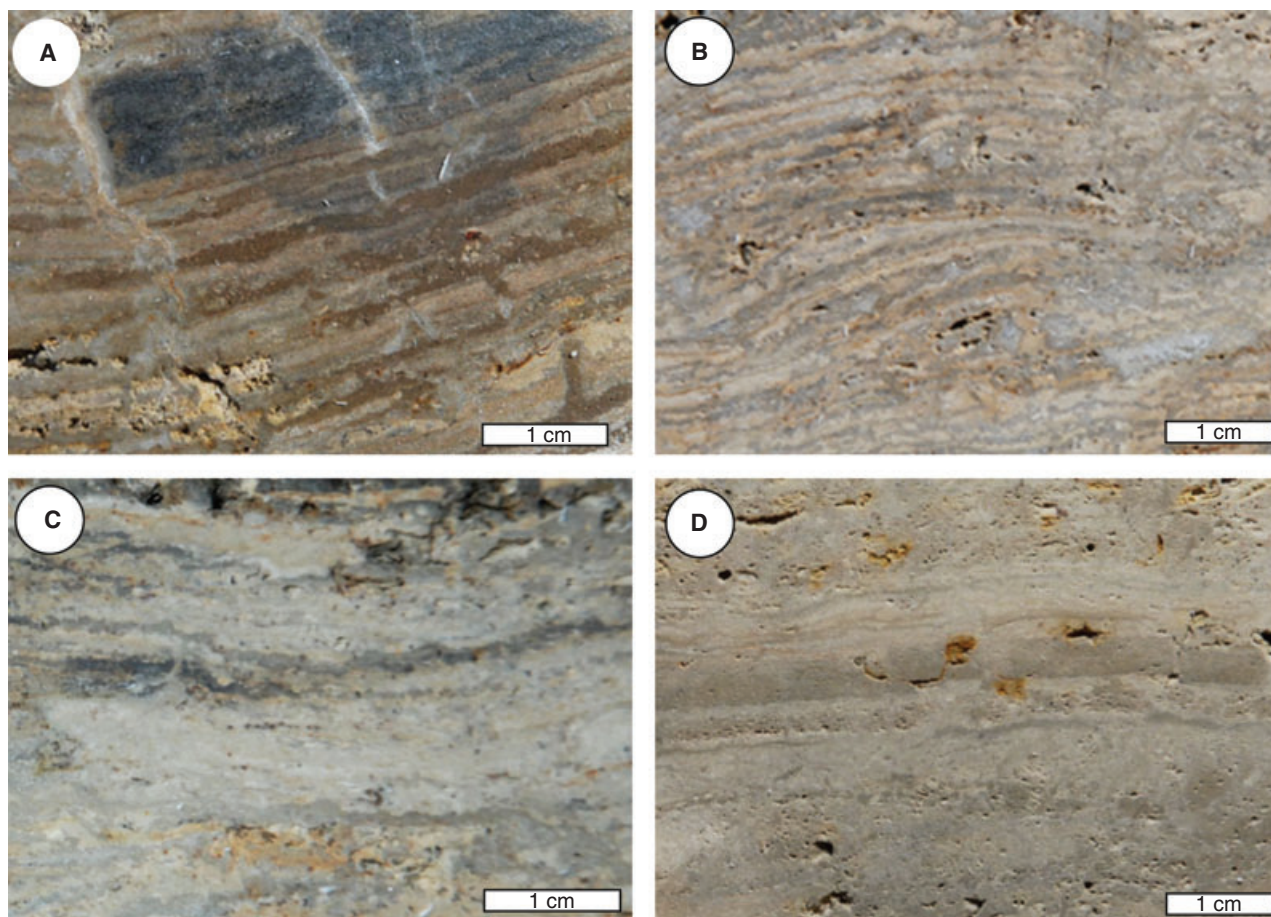


Fig. 3. Stromatolites. (A) Bottom bed showing irregular laminae (1.5 to 3 mm thick), grey–brown colour, local very low domes and evidence of intense bioturbation. (B) Middle bed with very thin brown and grey laminae, small open pores and domes up to 4.5 cm wide and 1.5 cm high. (C) Upper part of the middle bed, showing alternation of laminae interrupted by grey to dark–grey crinkly layers. (D) Top bed, showing laminae of variable thickness (1 to 5.5 mm), local very low domes, small fenestrae and vertical burrows.

aragonite and 72 h for dolomite. After reaction, CO_2 was cryogenically separated from the other gases and measured with a Finnigan Delta S mass spectrometer (Thermo Scientific, Dreieich, Germany). When both calcite/aragonite and dolomite were present, the techniques of Epstein *et al.* (1964) and Becker & Clayton (1972) were used. To allow for the different reaction rates of the carbonates, the CO_2 gas was collected at time intervals of 20 min for more reactive calcite and after 72 h for dolomite. The isotopic data are expressed in $\delta\text{‰}$ units and reported against the Pee Dee Belemnite (PDB-1) standard. The reproducibility for the isotopic determinations was $\pm 0.1\text{‰}$ for $\delta^{18}\text{O}$ and $\pm 0.05\text{‰}$ for $\delta^{13}\text{C}$.

Major and minor element concentrations were determined by X-ray fluorescence using a RIGAKU ZSX PRIMUS spectrometer (Rigaku International Corp., Osaka, Japan) on pressed, boric-acid backed pellets of bulk samples. Data reduction was achieved using the method

described by Franzini *et al.* (1975). Analytical errors were below 1% for Si and Al, below 3% for Fe and below 10% for Sr. Analyses for REE were carried out on 26 selected samples, via induced coupled mass spectrometry (ICP-MS), at Activation Laboratories Ltd (ActLabs; Ancaster, ON, Canada). For sample preparation, 0.5 g of bulk sample was acid-digested in the following stages: (i) hydrofluoric acid; (ii) a mixture of nitric and perchloric acids; (iii) dried using precise programmer controlled heating in several ramping and holding cycles; and (iv) brought back into solution using hydrochloric acid. The ICP-MS used was a Perkin Elmer Elan 6000 (Weltech Enterprises, Inc., Capitol Heights, MD, USA). The detection limit for REE (0.1 ppm) was that given by ActLabs. The abundance of REE was normalized to the average of North American, European and Russian shale composites adopted in many previous studies (Piper, 1974; Gromet *et al.*, 1984; Sholkovitz, 1988; Murray *et al.*, 1991).

Table 1. Mean values and variation ranges of carbonate mineralogy (%), carbonate stable isotopes ($\delta_{\text{‰}}$ versus PDB) and Sr concentrations (ppm) for lithologies from the Sutera section; n = sample number.

	Marls ($n = 20$)			Stromatolites ($n = 16$)			Dolostones ($n = 19$)			Aragonitic limestones ($n = 11$)			Claystones ($n = 13$)		
	Mean	Min	Max	Mean	Min	Max	Mean	Min	Max	Mean	Min	Max	Mean	Min	Max
Dolomite	28	2	64	78	43	99	85	43	99	3	3	3	4	2	6
Calcite	7	2	14	38	11	53	12	3	38	4	2	6	9	6	13
Aragonite	41	32	57	–	–	–	–	–	–	89	75	98	–	–	–
$\delta^{18}\text{O}_{\text{dolomite}}$	4.0	-0.8	7.6	6.6	4.1	7.9	5.7	4.1	7.9	–	–	–	–	–	–
$\delta^{13}\text{C}_{\text{dolomite}}$	-6.0	-12.2	0.3	-5.7	-11.3	-1.8	-7.7	-13.7	-1.3	–	–	–	–	–	–
$\delta^{18}\text{O}_{\text{Ca-carb}}$	-0.2	-0.2	-0.2	2.0	0.8	3.7	–	–	–	1.2	-0.2	2.5	–	–	–
$\delta^{13}\text{C}_{\text{Ca-carb}}$	1.8	1.8	1.8	-5.2	-31.6	-17.4	–	–	–	1.0	-0.1	1.9	–	–	–
Sr	819	128	5061	394	283	535	285	169	437	5795	5166	6922	414	89	1163

RESULTS AND INTERPRETATIONS

Mineralogy

X-ray diffraction analysis of bulk samples from the lower and middle part of the Sutera section shows dolomite as the predominant carbonate phase (up to 99%; Table 1). The marls contain between 2% and 64% dolomite, although in marly layers in the upper part of the section aragonite is the most abundant carbonate mineral. Stromatolite beds I and II (Fig. 2A) display dual carbonate mineralogy with dolomite ranging from 43% to 99% and calcite up to 53%. In stromatolite bed III (Fig. 2A), dolomite (mean value 97%) is the only carbonate present. The upper part of the section shows aragonite contents ranging from 32% to 98% (higher values in the aragonitic limestones), together with small percentages of calcite, dolomite (mean values of 4% and 3%, respectively) and celestite.

Clay minerals are present in variable proportions throughout the section, naturally being concentrated in the claystone levels (up to 85%) and generally being absent in stromatolites and aragonitic limestones. All samples contain detrital quartz with percentages being low in the carbonate layers (e.g. 0% to 4% in stromatolites) and higher (up to 60%) in the claystones.

Petrography

Textural features of stromatolites and aragonitic limestones

Carbonate in the first stromatolite bed (Figs 2A and 3A) occurs as millimetre-scale alternations of dense micrite and peloidal laminae. The peloidal laminae show: (i) fenestral pelsparite with irregular, locally dendritic, clumps of clotted micrite

(Fig. 4A); and (ii) pelmicrite/pelsparite including small peloids and disseminated pyrite. The stromatolites from the middle bed (Figs 2A, 3B and 3C) exhibit lamination resembling a dense felt preserved as dolomicrite that includes voids partially filled by calcite and, more rarely, by black amorphous matter (Fig. 4B and C). The third stromatolite bed (Figs 2A and 3D) consists of micrite in which fenestrae (generally 0.2 to 2 mm in size) alternate with irregular thin layers of dark wispy micrite (Fig. 4D). Both the lower and middle beds contain filaments *ca* 30 to 70 μm in width. In places the filaments appear fragmentary, but can be elongate and locally are distinctively recurved (Fig. 4B). Internally the filaments generally consist of dense micrite but can be traversed by light-coloured narrow transverse gaps (Fig. 4C).

Under the SEM untreated samples from the middle stromatolite bed show that the filaments are preserved in dolomicrite as a felted mass (Fig. 5A) in which individual filaments consist of rounded aggregates, each *ca* 40 μm in size, of dolomite crystals (Fig. 5B). The crystal faces locally show micron-sized rounded bodies partially incorporated or absorbed into the rhombohedral crystals (Fig. 5C). Biofilm-like remains are present in voids between filaments (Fig. 5D). Euhedral calcite crystals filling fenestral pores (Fig. 4A) locally have filamentous strands of branched material that may be organic, attached to and extending from the crystal faces (Fig. 6A).

Thin sections viewed by SEM show that the clotted dolomicrite exhibits surfaces marked with scars and black spots (Fig. 6B and C). The black spots appear as clusters enclosed within dolomicrite (Fig. 6C). In some cases, these spots are arranged as rings around dark rounded bodies (Fig. 6B). An enlarged view of the

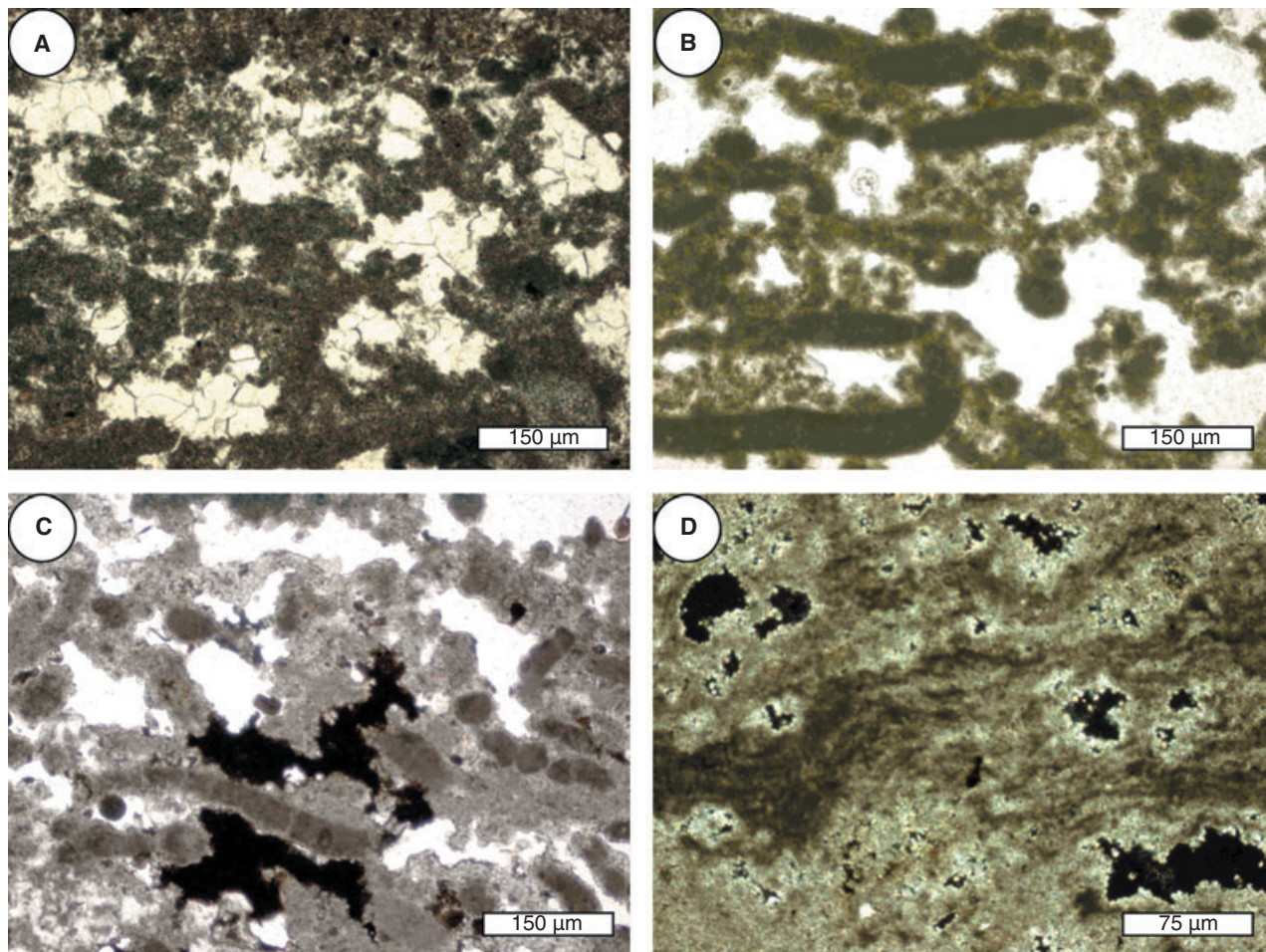


Fig. 4. Stromatolites in thin section. (A) Bottom bed, showing peloidal laminae and fenestral pelsparite with irregular, locally dendritic, clumps of clotted micrite (plane polarized light). (B) Middle bed, showing peloidal-clotted dolomicrite with fenestrae (partially filled by calcite) and recurved filaments (plane polarized light). (C) Middle bed, showing dolomicrite and filaments, with voids partially filled by black amorphous matter (plane polarized light). (D) Top bed with layers of dark thin wispy micrite and open fenestrae (crossed polars).

rounded bodies shows structures with a net-like fabric (Fig. 6D).

In SEM, the aragonitic limestones from the thick bed in the upper part of the section are seen to consist of a mass of needle-like aragonite crystals (Fig. 7A) of variable length. Generally, the needles are loosely packed and some of them form dumb-bell aggregates (Fig. 7B) similar to those reported in cold seep sites. The needles show preferential growth along their *c*-axis (Fig. 7B), typical of primary precipitation of aragonite (Gabrielli *et al.*, 1999).

Interpretation

The clotted–peloidal microfabrics in the stromatolite beds (Fig. 4) are typical of microbial carbonates (Riding, 2000) in which heterotrophic bacteria such as sulphate reducers degrade organic material (bacterial cells, extracellular

polymeric substances) within microbial mats, promoting calcification (Riding & Tomás, 2006). The filaments present in Sutura stromatolites resemble the large motile thiophilic bacterium *Beggiatoa*. Typically, *Beggiatoa* spp. use oxygen to oxidize sulphide to sulphate in sediments rich in hydrogen sulphide (Jørgensen & Revsbech, 1983). Since this reaction proceeds rapidly and spontaneously where oxygen is abundant, *Beggiatoa* only proliferates at the anoxic–oxic transition (Møller *et al.*, 1985). *Beggiatoa* uses its gliding ability to follow this chemical zone as it migrates during daily cycles in microbial mat microenvironments (Garcia-Pichel *et al.*, 1994). *Beggiatoa* mats can be unusually thick (>1 cm) in coastal-upwelling zones (Møller *et al.*, 1985) and at hydrothermal (Gundersen *et al.*, 1992) and methane seeps (Boetius & Suess, 2004). Filamentous cyanobacteria such as *Scytonema* (see

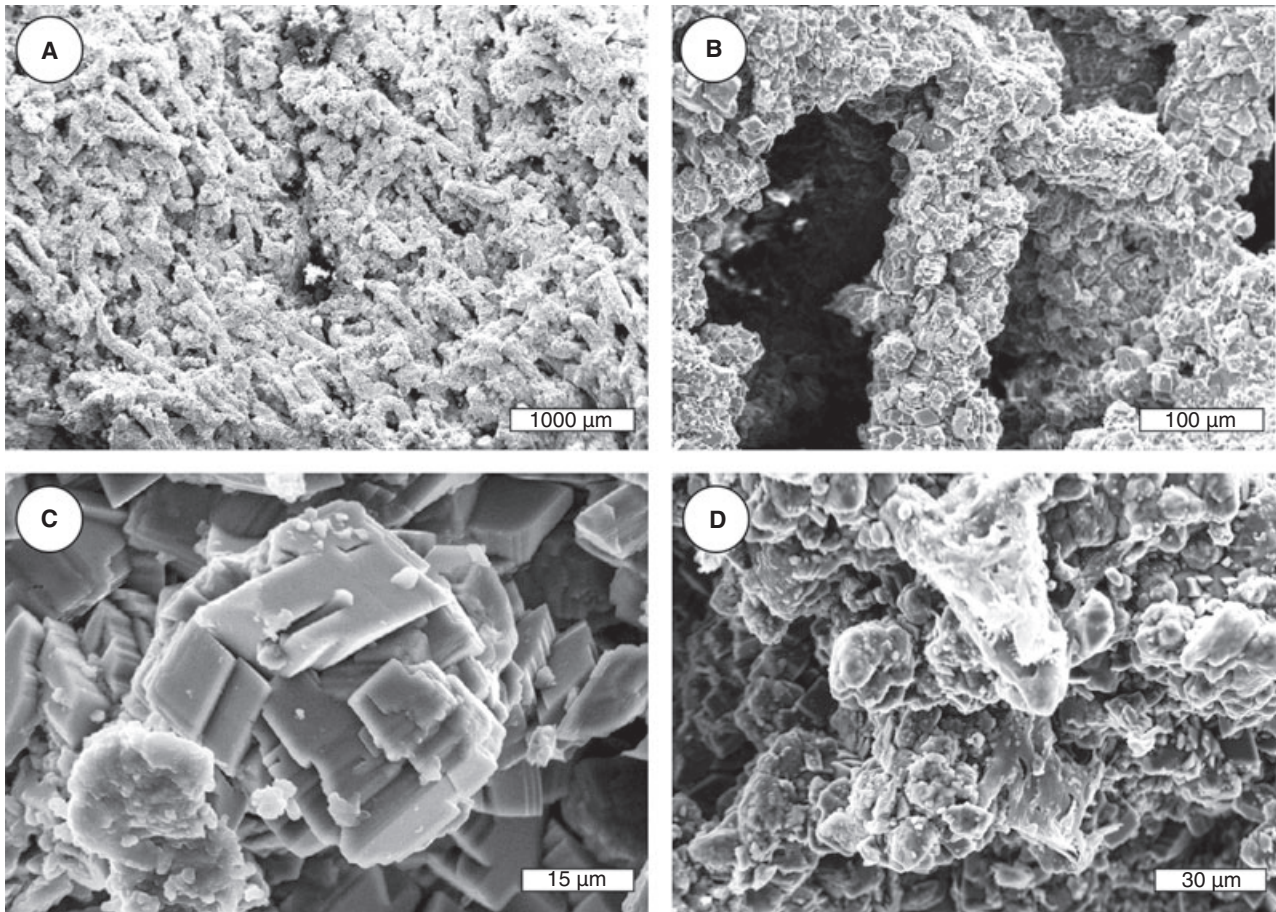


Fig. 5. SEM images of stromatolites (middle bed). (A) and (B) Dolomicrite preserving a felt-like mass of elongate filaments. (C) Spherical aggregates of dolomite crystals with micron-sized rounded shapes incorporated or absorbed into rhombohedral crystals. (D) Biofilm-like remains in voids between filaments.

Monty, 1965) have been reported in hypersaline settings (Vai & Ricci Lucchi, 1977; Rouchy & Monty, 1981). However, in size (diameter up to 70 µm) and dense felted arrangement the Sutera filaments (Figs 4 and 5) more closely resemble *Beggiatoa* or similar thiophilic bacteria. Similar filaments from a Tortonian methane seep in Central Italy have also been compared with *Beggiatoa* (Peckmann *et al.*, 2004; Fig. 2). In addition, the distinctively recurved shape of some of the Sutera filaments (Fig. 4B) recall the typical looping behaviour of present-day *Beggiatoa* as it reverses direction to avoid zones of elevated oxygen concentration (Møller *et al.*, 1985; Figs 4 and 8). Such abrupt chemotactic responses suggest relatively steep oxygen gradients (Møller *et al.*, 1985). This suggestion would be consistent with the very shallow-water environment inferred for the basal Calcare di Base at Sutera.

Recently, culture experiments have demonstrated that SRB are key players in dolomite

precipitation under sedimentary conditions (Warthmann *et al.*, 2000; Van Lith *et al.*, 2003; Wright & Wacey, 2005). The SRB degrade organic matter consuming sulphate and producing sulphide (H_2S), which can favour pyrite precipitation (FeS_2) when iron is available (Herbert *et al.*, 1998). The presence of disseminated pyrite in the dolomicrite could reflect SRB activity in Sutera stromatolites.

Biofilm-like alveolar structures in the dolomicrite (Fig. 6D) could suggest mineralization at the expense of organic material, such as extracellular polymeric substances (EPS), which contain organic templates that can act as carbonate mineral nucleation sites (Dupraz & Visscher, 2005). Also, the clusters of black spots floating in the dolomicrite mass (Fig. 5C) and the spherical aggregates of dolomite crystals (Fig. 6C) could reflect microbial carbonate precipitation. On the whole, the microtextural investigations suggest that the dolomite of Sutera stromatolites may have been strongly influenced by the metabolic

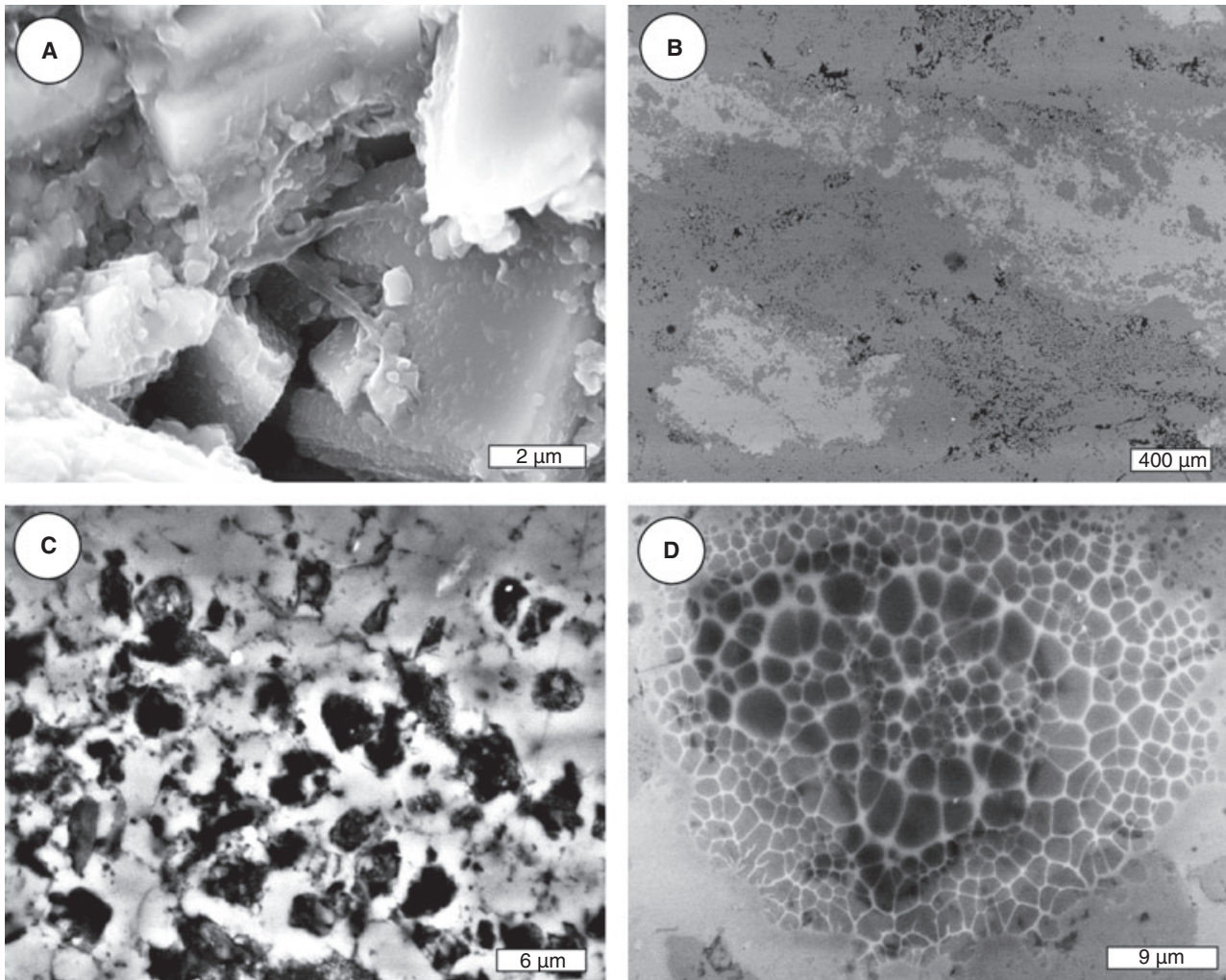


Fig. 6. SEM images of stromatolites (middle bed). (A) Euhedral calcite crystals filling fenestral pores and displaying strands of material that may be organic, attached to and extending from the crystal faces. (B) Dolomicrite surface marked by scars and black spots. (C) Black spot material enclosed within dolomicrite. (D) Detail of net-like fabric.

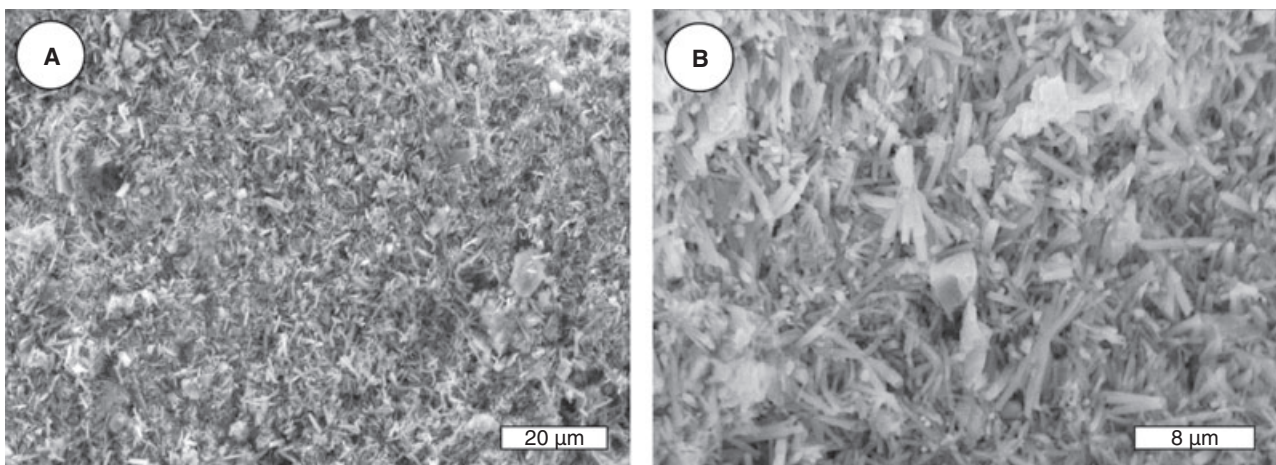


Fig. 7. SEM images of aragonitic limestone (thick bed). (A) Mass of needle-like aragonite crystals; (B) some of which form dumb-bell shaped aggregates.

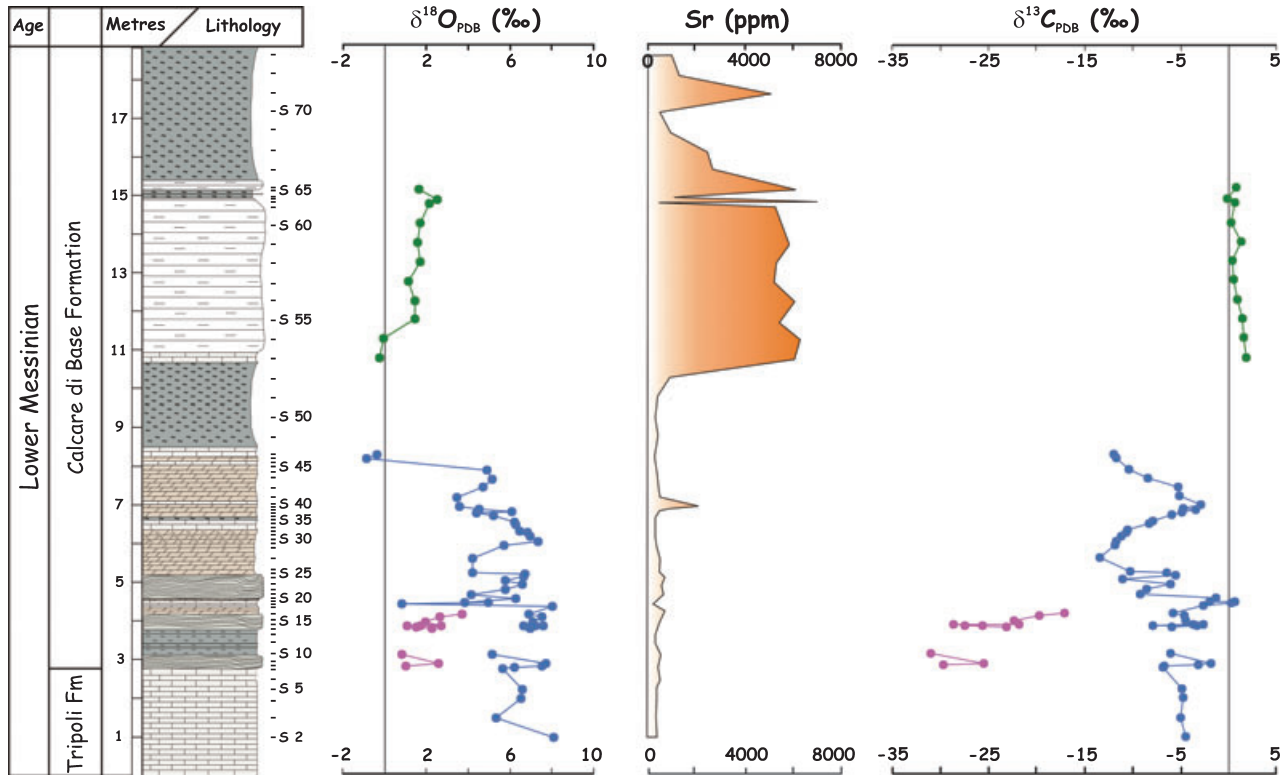


Fig. 8. Profiles of $\delta^{18}\text{O}$ ‰, Sr ppm and $\delta^{13}\text{C}$ ‰ for the Sutera section (lithological key as in Fig. 2), with sample mineralogy shown by colour: dolomite (blue), calcite (red) and aragonite (green).

activity of SRB and that EPS may have provided nucleation sites for dolomite precipitation.

Geochemistry

Stable oxygen and carbon isotopes

Dolomite from the Sutera section is characterized by high $\delta^{18}\text{O}$ values, generally between 4.1 and 7.9‰, and by a wide range of mostly negative $\delta^{13}\text{C}$ values from -13.7 ‰ to 0.3 ‰ (Fig. 8). A negative spike in the $\delta^{18}\text{O}$ dolomite curve (down to 0.8 ‰) marks the marly level intercalated between the II and III stromatolite beds. Near the transition to the first thick claystone level, oxygen and carbon isotope values of dolomite decline to -0.8 ‰ and -11.9 ‰, respectively. Calcite associated with dolomite from the stromatolite beds displays oxygen isotope values from 0.8 ‰ to 3.7 ‰ and is strongly depleted in ^{13}C , with values of -31.6 ‰ to -17.4 ‰.

In the upper portion of the section, essentially aragonitic carbonates exhibit isotopic composition in the ranges -0.2 ‰ $< \delta^{18}\text{O} < 2.5$ ‰ and -0.1 ‰ $< \delta^{13}\text{C} < 1.9$ ‰ (Fig. 8). Similar isotopic values were reported by Decima *et al.* (1988) for samples of aragonitic limestones from the same section.

Interpretation of isotope results

The relatively heavy $\delta^{18}\text{O}$ values of the dolomite (Fig. 8) reflect marine waters exposed to moderate to strong evaporation. The sudden decrease in $\delta^{18}\text{O}$ in the marly intercalation between the stromatolite beds is interpreted as evidence of a brief dilution event. The negative $\delta^{13}\text{C}$ values of the Sutera dolomite (down to -13.7 ‰) suggest large availability of organic, isotopically light carbon in dolomite-forming waters, implying organic matter degradation processes probably favoured by periods of increased stagnation. The negative shifts in both oxygen and carbon isotope values towards the mid-part of the section (Fig. 8) suggest dilution of evaporated marine waters by continental runoff.

Although previous studies give conflicting results regarding differential oxygen isotope fractionation during the precipitation of carbonate minerals (Land, 1980; McKenzie, 1981; Schmidt *et al.*, 2005), the *ca* 5‰ lower $\delta^{18}\text{O}$ values of calcites from the Sutera section in comparison to coexisting dolomites suggest that the two minerals were not strictly cogenetic and reflect differing temperature and more dilute water during crystallization. This is consistent with petrographic observations indicating an early diagenetic origin

for the calcite. The extremely negative $\delta^{13}\text{C}$ values of the same calcites (from -17.4 down to -31.6% ; Fig. 8, Table 1) might indicate a methane carbon source for this carbonate.

The isotopic compositions of the aragonitic limestones are in the range of carbonates formed from normal to slightly evaporated marine waters. Even taking into account possible effects of aragonite–dolomite isotope fractionation, the shift in the $\delta^{18}\text{O}$ curve near the beginning of aragonite precipitation is large enough to indicate a change in depositional conditions in the Sutera basin.

Overall, the isotopic data support the view that the variation in carbonate mineralogy through the Sutera section reflects evolution from strongly evaporated marine waters (in which the stromatolites formed) to normal or slightly evaporated marine waters (in which the aragonitic limestones formed). Deposition probably occurred in a semi-closed marine environment subject to wide variations in salinity related to episodes of meteoric water influx (see Guido *et al.*, 2007).

Sr distribution

Mean values and ranges of Sr concentrations in Sutera lithologies are listed in Table 1. The vertical log of Sr data shows two clearly distinct parts: low values in the lower half of the section, followed by an abrupt increase that is sustained through the upper half of the section (Fig. 8). The rise in concentrations (up to 6922 ppm; Table 1) commences at the transition to the aragonitic limestones in the upper portion of the section. Dolomite-rich carbonates (i.e. stromatolites and dolostones) from the lower part of the section have a mean Sr concentration of 340 ppm. The stromatolites fall within the range from 283 to 535 ppm (Table 1).

Interpretation of Sr results

High Sr/Ca ratios in carbonate sediments are inferred to correspond to aragonite enrichment (Azzaro *et al.*, 1993; Thomson *et al.*, 2004) and Sr concentrations in the Sutera section reflect the abundance of aragonite (Fig. 8). Incorporation of Sr^{2+} into aragonite appears to be independent of salinity (Gaetani & Cohen, 2006), and aragonitic limestones from the Sutera section show Sr concentration values (up to 6922 ppm; Table 1) that are similar to those commonly reported for aragonite precipitated from normal marine waters (8300 ppm, Kinsman, 1969; 9000 ppm, Bathurst, 1975). Dolomite-rich carbonates (i.e. stromatolites and dolostones) from the lower part of the section

exhibit a mean Sr concentration of 340 ppm. This is lower than the Sr content of marine to hypersaline dolomites (*ca* 600 ppm, Behrens & Land, 1972; 500 to 800 ppm, Land, 1980) but higher than that reported for ancient marine or marine–meteoric dolomites (generally < 200 ppm, Machel & Anderson, 1989). As a whole, these Sr concentration data support the interpretation of the stable isotope results in terms of a transition of the Sutera depositional environment from strongly evaporated to normal or slightly evaporated conditions, with dolomites generally recording evaporative episodes.

Rare earth elements

The main compositional data of REE + Y in the stromatolite samples and, for comparison, in the dolostones, aragonitic limestones and claystones/marls from the Sutera section are shown in Table 2. Stromatolites have the lowest total REE (ΣREE) concentrations, whereas the aragonitic limestones and claystones/marls display higher ΣREE values probably due to the presence of more abundant REE-rich terrigenous components (Table 2). Dolostones overlying the stromatolites exhibit intermediate values. La_n/Yb_n ratios of the stromatolites are > 1 , indicating moderate enrichment in light REE (LREE) compared to heavy REE (HREE) in contrast to marine carbonate that is typically LREE-depleted. In addition, the stromatolites are slightly enriched in LREE relative to middle REE (MREE) ($\text{La}_n/\text{Sm}_n = 1.1$ to 1.5 , $\text{Pr}_n/\text{Sm}_n = 1.0$ to 1.3 ; Table 2) and, at least for some samples, slightly depleted in HREE relative to MREE ($\text{Dy}_n/\text{Yb}_n =$ up to 1.6 ; Table 2).

REE interpretations

The estimation of sea water chemistry in the geological past is dependent upon sedimentary proxies (e.g. directly precipitated evaporites) thought to reliably reflect contemporaneous sea water composition, based on studies of elements with known and predictable behaviour in modern sea water and their fractionation in modern sea water precipitates. Sedimentary records of REE have been used widely to derive palaeo-sea water REE patterns, although the stability of these elements during burial and diagenesis is still a matter of discussion (Banner *et al.*, 1988; McLennan, 1989; Holser, 1997; Webb & Kamber, 2000; Shields & Webb, 2004) and REE fractionation may occur during marine mineral precipitation. However, owing to their tendency to incorporate REE from sea water with uniform and high partition coefficients, microbial carbonates are currently

Table 2. REE + Y composition (ppm) and shale-normalized REE index ratios of samples from the Sutera section grouped according to lithology; nd = not detected.

Sample	La	Ce	Pr	Nd	Sm	Eu	Gd	Tb	Dy	Y	Ho	Er	Tm	Yb	ΣREE	La _n /Yb _n	La _n /Sm _n	Pr _n /Sm _n	Dy _n /Yb _n	Pr _n /Nd _n
Stromatolites																				
S 24	2·4	3·6	0·6	2	0·4	0·10	0·4	nd	0·3	2·0	nd	0·2	nd	0·2	10·2	1·03	1·10	1·11	0·96	1·13
S 23	1·8	2·7	0·4	1·5	0·3	0·07	0·3	nd	0·3	1·6	nd	0·1	nd	nd	7·6	nd	1·10	0·99	nd	1·00
S 21	3·5	6·3	0·8	2·9	0·6	0·11	0·5	nd	0·5	2·6	nd	0·3	nd	0·2	15·7	1·50	1·07	0·99	1·60	1·04
S 16	4·1	7·8	1·0	3·3	0·7	0·13	0·5	nd	0·4	2·6	nd	0·3	nd	0·2	18·4	1·75	1·07	1·06	1·28	1·14
S 15d	2·7	4·2	0·6	2·1	0·4	0·09	0·4	nd	0·3	1·7	nd	0·2	nd	0·2	11·2	1·16	1·23	1·11	0·96	1·07
S 15c	3·6	6·3	0·9	2·7	0·6	0·13	0·4	nd	0·4	2·0	0·1	0·2	nd	nd	15·4	nd	1·10	1·11	nd	1·25
S 15b	2·9	4·8	0·7	2·2	0·4	0·08	0·4	nd	0·3	2·0	nd	0·2	nd	0·2	12·2	1·24	1·33	1·30	0·96	1·20
S 15a	1·9	3·1	0·4	1·5	0·3	0·07	0·3	nd	0·3	1·6	nd	0·1	nd	nd	8·1	nd	1·16	0·99	nd	1·00
S 14	2·4	3·7	0·5	1·7	0·3	0·07	0·3	nd	0·3	1·8	nd	0·1	nd	nd	9·5	nd	1·46	1·24	nd	1·11
S 08	4·3	7·1	1·0	3·6	0·7	0·15	0·7	nd	0·6	3·7	0·1	0·3	nd	0·3	18·9	1·23	1·12	1·06	1·28	1·04
Dolostones																				
S 44	4·8	8·8	1·1	3·7	0·8	0·14	0·7	nd	0·6	3·3	0·1	0·3	nd	0·3	21·3	1·37	1·10	1·02	1·28	1·12
S 42	13·4	20·8	3·0	11·5	2·4	0·51	2·2	0·3	1·7	11·3	0·4	1·1	0·2	1·0	58·7	1·15	1·02	0·93	1·09	0·98
S 38	4·7	7·5	1·1	4·2	1·0	0·25	1·1	0·2	1·0	6·5	0·2	0·6	nd	0·4	22·2	1·01	0·86	0·82	1·60	0·98
S 36	7·9	15·4	1·8	6·9	1·6	0·37	1·6	0·2	1·4	7·8	0·3	0·7	nd	0·6	38·6	1·13	0·90	0·83	1·49	0·98
S 29	11·4	18·8	2·8	9·9	2·1	0·43	1·8	0·3	1·5	8·2	0·3	0·9	0·1	0·8	51·2	1·22	0·99	0·99	1·20	1·06
S 27	3·5	6·1	0·8	3·1	0·6	0·13	0·6	nd	0·5	3·3	nd	0·3	nd	0·2	15·8	1·50	1·07	0·99	1·60	0·97
Aragonitic limestones																				
S 63	16·8	33·6	4·0	15·0	2·9	0·61	2·6	0·3	2·1	14·4	0·4	1·3	0·2	1·2	81·1	1·20	1·06	1·02	1·12	1·00
S 61	14·5	22·6	3·4	12·7	2·8	0·60	2·5	0·4	2·3	13·8	0·5	1·4	0·2	1·3	65·4	0·95	0·95	0·90	1·13	1·01
S 57	11·1	17·8	2·7	9·9	2·4	0·57	2·5	0·4	2·2	12·4	0·4	1·2	0·2	0·9	52·4	1·06	0·85	0·83	1·56	1·03
S 54	33·3	67·1	7·7	29·6	5·6	1·18	4·6	0·6	3·0	15·7	0·5	1·4	0·2	1·0	155·8	2·85	1·09	1·02	1·92	0·98
Claystones/marls																				
S 70	28·7	47·3	7·5	27·7	5·9	1·19	4·9	0·7	4·1	20·4	0·8	2·3	0·3	2·1	133·8	1·17	0·89	0·94	1·25	1·02
S 64	30·4	55·8	7·6	27·5	5·2	1·10	4·5	0·6	3·5	18·3	0·7	2	0·3	1·8	141·2	1·45	1·07	1·08	1·24	1·04
S 49	15·1	27·7	4·4	16·0	3·4	0·68	2·8	0·4	2·4	9·6	0·5	1·5	0·2	1·4	76·7	0·92	0·81	0·96	1·09	1·03
S 34	24·7	39·9	5·5	20·5	4·1	0·82	3·4	0·5	2·6	15·8	0·5	1·5	0·2	1·3	105·7	1·63	1·10	1·00	1·28	1·01
S 18	36·5	57·8	9·1	33·9	7·1	1·47	5·7	0·8	4·7	23·6	0·9	2·7	0·4	2·3	163·7	1·36	0·94	0·95	1·31	1·01
S 04	29·7	47·1	6·8	25·3	5·2	1·10	4·6	0·6	3·8	22·9	0·8	2·2	0·3	1·9	129·7	1·34	1·04	0·97	1·28	1·01

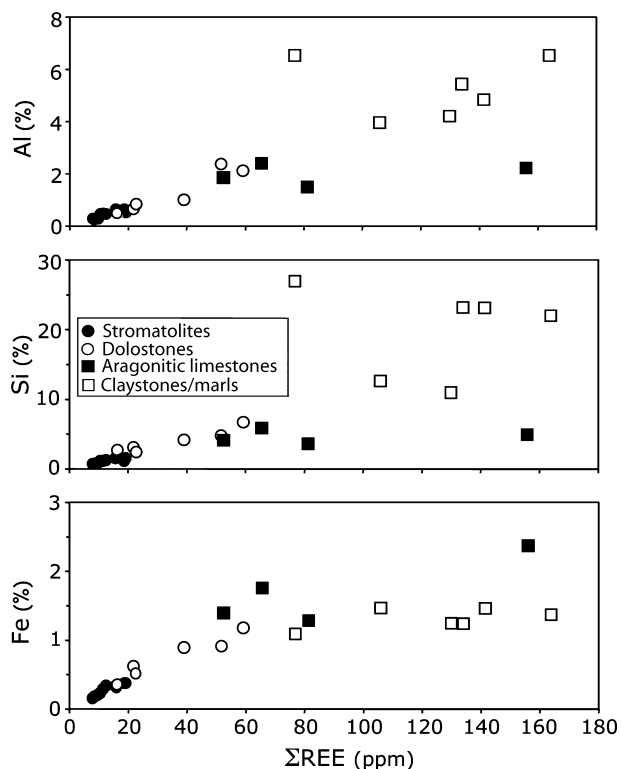


Fig. 9. Cross-plots of Al, Si and Fe (%) versus Σ REE (ppm) for Sutera stromatolites, dolostones, aragonitic limestones and claystones/marls.

considered to be reliable proxies for reconstruction of ancient sea water REE geochemical signatures (Webb & Kamber, 2000; Olivier & Boyet, 2006). Fractionation patterns of dissolved REEs in present-day oceans typically show low REE concentrations, with HREEs > LREEs, and a distinct 'Ce-anomaly' (German & Ederfield, 1990). Negative Ce anomalies reflect oxidation of Ce^{3+} to Ce^{4+} , reducing its solubility (Moffett, 1990, 1994; Sholkovitz & Schneider, 1991; DeCarlo *et al.*, 1998).

In interpreting REE data, it is necessary to consider detrital contamination that could effectively mask a sea water signature in the carbonates due to the much larger REE concentration and shale-like REE signature of terrigenous materials ('flat pattern'; German & Ederfield, 1990; Bau & Dulski, 1996; Byrne *et al.*, 1996; Webb & Kamber, 2000). Carbonate samples with <1 to 2% shale contamination may be representative of the water composition from which they precipitated (Nothdurft *et al.*, 2004).

For the Sutera samples, Σ REE correlates well with elements representative of fine-grained and sand-sized detritus, such as Al and Si (Fig. 9). A significant correlation also occurs between Σ REE and Fe concentrations. Point distributions in Fig. 9 suggest that the detrital contribution of

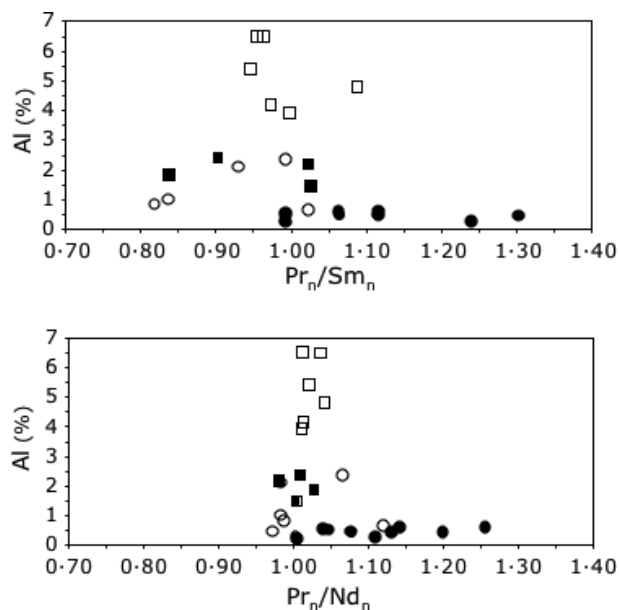


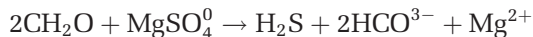
Fig. 10. Cross-plots of Al (%) versus Pr_n/Sm_n and Pr_n/Nd_n ratios for Sutera stromatolites, dolostones, aragonitic limestones and claystones/marls (key as in Fig. 9).

REE, carried by clay minerals or Fe oxyhydroxides, progressively and significantly decreases from claystones/marls to aragonitic limestones, dolostones and stromatolites. The stromatolites seem to have been only slightly affected by detrital contamination. Moreover, it is to be noted that parameters expressing relative REE concentrations, such as Pr_n/Sm_n and Pr_n/Nd_n , do not correlate with Al (Fig. 10), Fe and Σ REE (the last two are not shown in the figure). This suggests that factors other than detrital contamination largely determine the Sutera REE distribution.

DISCUSSION

Microbial activity can account for many of the microfabrics observed in the Sutera stromatolites, in which dolomite is the dominant carbonate. Based on petrographic observations, this dolomite is not replacive and is inferred to be a primary precipitate. It is proposed that dolomite which preserves the microbial filaments and which consists of rounded crystal aggregates (Fig. 5B and C) formed, at least in the nucleation phase, through bacterial mediation, which helped to overcome kinetic inhibitors. Based on results of laboratory experiments and sediment investigations, various authors have suggested that BSR overcomes kinetic barriers to dolomite precipitation by removing sulphate, reducing

the solubility of Mg^{2+} and Ca^{2+} ions, increasing pH and carbonate alkalinity and providing nucleation sites for carbonate precipitation (Compton, 1988; Vasconcelos & McKenzie, 1997; Warthmann *et al.*, 2000; Van Lith *et al.*, 2003; Wright & Wacey, 2005). Sulphate-reducing bacteria can remove sulphate and release Mg^{2+} in the solution from $MgSO_4^0$, according to:



This reaction is accompanied by pyrite precipitation ('disseminated pyrite in dolomicrite', see *Petrography* section above) and NH_3 produced bacterially (Berner, 1980). The ammonia, which is highly soluble, increases the pH of the microenvironment via generation of hydroxide and produces higher levels of alkalinity that favour dolomite precipitation. This process requires the presence of organic matter utilized by the bacteria as an energy source. The organic matter can be derived from cellular material and cell products, such as EPS. Progressive consumption of organic matter by heterotrophic bacteria, including SRB, can result in localized carbonate precipitation. In the Sutera samples, this could account for the clotted–peloidal dolomicrite (Fig. 4A) and partially preserved biofilm-like structure in dolomicrite (Fig. 5D).

Consistent with this view, primary precipitation may have formed micron-sized rounded shapes (see Fig. 5B and C) that were subsequently incorporated or absorbed into rhombohedral dolomite. Similar structures in dolomites from the Coorong region have been interpreted as diagenetic self-organisation of mineral grains driven by neomorphism (Wright, 1999). In the Sutera stromatolites, bacterial-mediated precipitation produced clotted dolomicrite with micropeloids and fenestral pores (Fig. 4B and C) that opened between the micrite and micropeloids, due to shrinkage of degrading organic matter (cf. Riding & Tomás, 2006). During a subsequent, but still early, diagenetic phase, sparry calcite cement filled fenestral pores (Fig. 4A).

Plotting $\delta^{18}O$ versus $\delta^{13}C$ data of carbonates from the stromatolite beds shows that the dolomite and associated calcite occupy two distinct fields (Fig. 11). High $\delta^{18}O$ dolomite values (up to 7.9‰), similar to those of well-known modern dolomites from ephemeral lakes of the Coorong region in Australia (Rosen *et al.*, 1989), are consistent with precipitation under hypersaline environmental conditions. Under these conditions, and those at Sutera, $\delta^{13}C$ values are liable to be subject to a variety of influences, such as buffering of pore

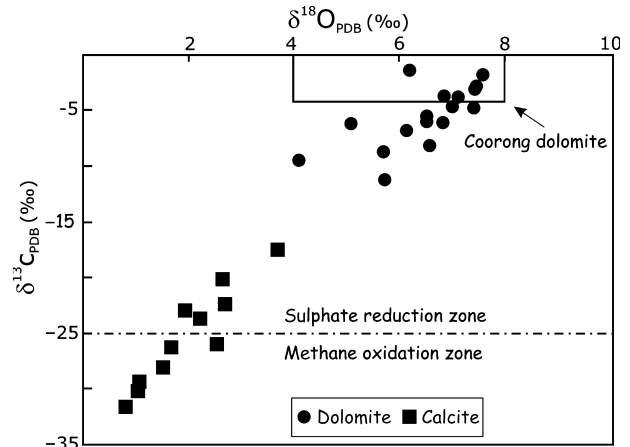


Fig. 11. $\delta^{13}C$ versus $\delta^{18}O$ cross-plot for stromatolite carbonates. The rectangle at the top indicates isotope compositions of dolomites from ephemeral lakes of the Coorong Region (data from Rosen *et al.*, 1989).

water values (Walter *et al.*, 1993), variations in diffusive fluxes (Boehme *et al.*, 1996) and differences in metabolic pathways (Goevert & Conrad, 2008). Even under hypersaline conditions, Sutera carbon isotope values of ca -5‰ (Fig. 11) strongly suggest organically derived carbon. This interpretation is reinforced by the presence of even more negative $\delta^{13}C$ values (down to -11.3‰) of the dolomites. It is therefore inferred that these dolomite precipitates reflect strong organic activity consistent with bacterial mediation.

With regard to the very negative carbon isotopic signatures of calcite, inferred here to possibly reflect a methane carbon source (see above), numerous studies have documented the geochemical evidence for microbial production and oxidation of methane in marine sediments (citations in Magonigal *et al.*, 2003). Kinetic effects on carbon during CH_4 production and oxidation tend to concentrate the lighter ^{12}C isotope in the resulting CO_2 (Barker & Fritz, 1981; Whiticar *et al.*, 1986) and in the carbonates that can form. On the other hand, the very negative $\delta^{13}C$ values of calcite (down to -31.6‰; see Fig. 8) suggest that microbial communities may have promoted calcite precipitation through methane oxidation, using sulphate as the electron acceptor according to the following net equation (Barnes & Goldberg, 1976; Reeburgh, 1976; Iversen & Jørgensen, 1985):



As reported before, contemporaneous occurrence of methanogenesis and anaerobic oxidation of methane has been observed in modern sediments (Orcutt *et al.*, 2005). A distinctive feature of the

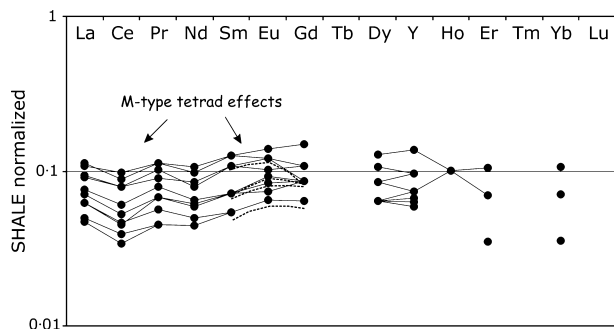


Fig. 12. Shale-normalized REE + Y patterns for Sutera stromatolites. Note the convex curved segments (tetrad effect, dotted curves) and the peaks around Sm and Eu (MREE).

REE_n patterns for the Sutera section is that the Pr_n/Sm_n ratios are >1 for most stromatolite samples, and generally <1 for the other lithologies (Fig. 10), emphasizing LREE enrichment in the stromatolites. Similar enrichments have been reported by Tlig & M'Rabet (1985) for dolomites from sabkha environments and ascribed to the influence of inorganic complexes that increase solubility of the heavy REE in basic solutions, with respect to the lighter elements of the REE group. However, evaporitic dolomites from non-stromatolite strata in the Sutera section display Pr_n/Sm_n ≤ 1. Enrichment of LREE is observed in present-day microbialites (Webb & Kamber, 2000) and Upper Jurassic (Olivier & Boyet, 2006) microbial carbonates, and in Miocene organogenic dolomites (Miller & Leybourne, 2003).

In a study of REE adsorption onto bacterial cell walls, Takahashi *et al.* (2005) attributed enrichment around Pr to the tetrad effect, resulting in REE_n patterns that no longer increase or decrease smoothly with ionic radius but instead show internal irregularities. The tetrad effect refers to convex curves (M-type tetrad effect; Masuda *et al.*, 1987) that appear in four regions of the REE_n pattern: La–Ce–Pr–Nd, (Pm)–Sm–Eu–Gd, Gd–Tb–Dy–Ho and Er–Tm–Yb–Lu (Peppard *et al.*, 1969; Jørgensen, 1970; Nugent, 1970; Masuda & Ikeuchi, 1979; Kawabe, 1992; Bau, 1996). Takahashi *et al.* (2005) recognized the tetrad effect particularly in the first two tetrads and ascribed it to REE forming inner sphere complexes during their adsorption onto bacteria.

In many of the stromatolite samples from Sutera, the second tetrad is prominent and readily recognizable as a convex curved segment (M-type tetrad effect; Fig. 12). A similar trend, with a peak around Sm and Eu (MREE), is reported by Takahashi *et al.* (2007) for distribution patterns related to complexing sites at the bacterial surface. The

first tetrad is poorly defined, due to a negative anomaly for redox-sensitive Ce. However, there is enrichment in Pr accompanied by a decline in Nd (Pr_n/Nd_n from 1 to 1.25; Fig. 10), which is typical of the first tetrad (Takahashi *et al.*, 2005). These observations of Sutera stromatolites, consistent with their petrography and isotope geochemistry, strengthen the view that distinctive LREE enrichment together with the tetrads observed in the REE patterns can provide geochemical signatures of past bacterial activity.

CONCLUSION

During deposition of the basal part of the Messinian Calcare di Base at Sutera, shallow hypersaline marine conditions favoured the establishment of microbial mat communities with *Beggiatoa*-like filaments and heterotrophs such as sulphate-reducing bacteria. The dolomite appears to be persistently linked to bacterial sulphate reduction (BSR). Co-occurrence of early dolomitized bacterial filaments and negative δ¹³C values could indicate BSR that promoted carbonate precipitation and provided H₂S for thiophilic bacteria. In this view, the carbonate composition, dolomite mineralogy, microfabrics (clotted, peloidal) and microfossils (*Beggiatoa*-like filaments) of the Sutera stromatolites are intimately linked. Consistent with the petrography and geochemical signatures of the stromatolites, including a distinctive light rare earth element (LREE) enrichment and tetrads in the REE patterns, it is suggested that bacterial biomineralization processes had a major role in carbonate precipitation within these deposits. On this basis, stable (C and O) isotopes and REE patterns from microbial carbonates can provide a reliable source of information on the chemistry of ancient marine sedimentary environments.

ACKNOWLEDGEMENTS

We thank J.P. Calvo for his helpful comments on a preliminary version of the manuscript. Sedimentology reviewers C.B. Schreiber and D.T. Wright critically read the manuscript and made helpful suggestions. Thanks are also due to E. Curcuruto for assistance during a preliminary sampling of the Sutera section, and to G. Capasso and F. Grassa (INGV, Palermo) for facilitating stable isotope analysis. The International Association of Sedimentologists (IAS) sponsored EO's participation in EGU 2006. EO's PhD research was

supported by the European Social Fund. Additional financial support was provided by a MIUR (ex-quota 60%) Grant to RN.

REFERENCES

- Azzaro, E., Bellanca, A. and Neri, R.** (1993) Mineralogy and geochemistry of Mesozoic black shales and interbedded carbonates, southeastern Sicily: evaluation of diagenetic processes. *Geol. Mag.*, **130**, 191–202.
- Banner, J.L., Hanson, G.N. and Meyers, W.J.** (1988) Rare earth element and Nd isotopic variations in regionally extensive dolomites from the Burlington-Keokuk Formation Mississippian; implications for REE mobility during carbonate diagenesis. *J. Sed. Petrol.*, **58**, 415–432.
- Barahona, E., Huertas, F., Pozzuoli, A. and Linares, J.** (1982) Mineralogia e genesi dei sedimenti della provincia di Granada (Spagna). *Miner. Petrogr. Acta*, **26**, 61–90.
- Barker, J.F. and Fritz, P.** (1981) Carbon isotope fractionation during microbial methane oxidation. *Nature*, **293**, 289–291.
- Barnes, R.O. and Goldberg, E.D.** (1976) Methane production and consumption in anaerobic marine sediments. *Geology*, **4**, 297–300.
- Bathurst, R.G.C.** (1975) *Carbonate Sediments and Their Diagenesis*, 2nd edn. Elsevier, Amsterdam, The Netherlands, 658 pp.
- Bau, M.** (1996) Control on the fractionation of isoivalent trace elements in magmatic and aqueous systems: evidence from Y/Ho, Zr/Hf, and lanthanide tetrad effect. *Contrib. Mineral. Petrol.*, **123**, 323–333.
- Bau, M. and Dulski, P.** (1996) Distribution of yttrium and rare-earth elements in the Penge and Kuruman iron-formations, Transvaal Supergroup, South Africa. *Precambrian Res.*, **79**, 37–55.
- Becker, R.H. and Clayton, R.N.** (1972) Carbon isotopic evidence for the origin of a banded iron-formation in western Australia. *Geochim. Cosmochim. Acta*, **36**, 577–596.
- Behrens, E.W. and Land, L.S.** (1972) Subtidal Holocene dolomite, Baffin Bay, Texas. *J. Sed. Petrol.*, **42**, 155–161.
- Bellanca, A. and Neri, R.** (1986) Evaporite carbonate cycles of the Messinian, Sicily: stable isotopes, mineralogy, textural features, and environmental implications. *J. Sed. Petrol.*, **56**, 614–621.
- Bellanca, A., Calderone, S. and Neri, R.** (1983) Evidenze geochemiche e mineralogiche di episodi evaporitici nella sequenza diatomitica (Messiniano pre-evaporitico) di Sutura (Sicilia centrale), *Rend. Soc. Ital. Miner. Petrol.*, **38**, 1271–1280.
- Bellanca, A., Calderone, S. and Neri, R.** (1986) Isotope geochemistry, petrology and depositional environments of the diatomite-dominated Tripoli Formation (Lower Messinian), Sicily. *Sedimentology*, **33**, 729–743.
- Bellanca, A., Caruso, A., Ferruzza, G., Neri, R., Rouchy, J.M., Sprovieri, M. and Blanc-Valleron, M.M.** (2001) Transition from marine to hypersaline conditions in the Messinian Tripoli Formation from the marginal areas of the central Sicilian Basin. *Sed. Geol.*, **140**, 87–105.
- Berner, R.A.** (1980) *Early Diagenesis: A Theoretical Approach*. Princeton University Press, Princeton, NJ.
- Boehme, S.E., Blair, N.E., Jeffrey, L., Chanton, P. and Martens, C.S.** (1996) A mass balance of ^{13}C and ^{12}C in an organic-rich methane-producing sediment. *Geochim. Cosmochim. Acta*, **60**, 3835–3848.
- Boetius, A. and Suess, E.** (2004) Hydrate Ridge: a natural laboratory for the study of microbial life fuelled by methane from near-surface gas hydrates. *Chem. Geol.*, **205**, 291–310.
- Butler, R.W.H., Lickorish, W.H., Grasso, M., Pedley, H.M. and Ramberti, L.** (1995) Tectonics and sequence stratigraphy in Messinian basins, Sicily; constraints on the initiation and termination of the Mediterranean salinity crisis. *Geol. Soc. Am. Bull.*, **107**, 425–439.
- Butler, R.W.H., McClelland, E. and Jones, R.E.** (1999) Calibrating the duration and timing of the Messinian salinity crisis in the Mediterranean: linked tectonoclimatic signals in thrust-top basins of Sicily. *J. Geol. Soc. London*, **156**, 827–835.
- Byrne, R.H., Liu, X. and Schuf, J.** (1996) The influence of phosphate coprecipitation on rare earth distributions in natural waters. *Geochim. Cosmochim. Acta*, **60**, 3341–3346.
- Canfield, D.E. and Des Marais, D.J.** (1991) Aerobic sulfate reduction in microbial mats. *Science*, **51**, 1471–1473.
- Caruso, A., Di Stefano, E., Rouchy, J.M. and Sprovieri, R.** (1997) Biostratigraphy, cyclostratigraphy and sedimentology controls of the transition Tripoli-Calcare di Base (Lower Messinian) from Caltanissetta Basin (Sicily). *Eighth Workshop of the ILP Task Force, Origin of Sedimentary Basins*, Palermo, Abstr.
- Castanier, S., Le Métayer-Levrel, G. and Perthuisot, J.-P.** (2000) Bacterial roles in the precipitation of carbonate minerals. In: *Microbial Sediments* (Eds R.E. Riding and S.M. Awramik), pp. 32–39, Springer, Berlin.
- Cavazza, W. and Wezel, F.C.** (2003) The Mediterranean region – a geological primer. *Episodes*, **26**, 160–168.
- Cita, M.B.** (1975) The Miocene-Pliocene boundary: history and definition. In: *Late Neogene Epoch Boundaries* (Eds T. Saito and L.H. Burkle), Micropaleontology Press, *Spec. Publ.*, **1**, 1–30.
- Cita, M.B. and Colombo, L.** (1979) Sedimentation in the latest Messinian at Capo Rossello (Sicily). *Sedimentology*, **26**, 497–522.
- Cita, M.B., Wright, R.C., Ryan, W.B.F. and Longinelli, A.** (1978) Messinian paleoenvironments. In: *Initial Reports of the Deep Sea Drilling Project* (Eds K.J. Hsü, L. Montadert, R.B. Garrison, F.H. Fabricius, R.B. Kidd, C. Müller, M.B. Cita, G. Bizon, R.C. Wright, A.E. Erickson, D. Bernoulli and F. Mélières), Vol. 42, Part 1, pp. 1003–1035. US Government Printing Office, Washington.
- Clauzon, G., Suc, J.P., Gautier, F., Berger, A. and Loutre, M.F.** (1996) Alternate interpretation of the Messinian Salinity Crisis; controversy resolved? *Geology*, **24**, 363–366.
- Claypool, G.E. and Kaplan, I.R.** (1974) The origin and distribution of methane in marine sediments. In: *Natural Gases in Marine Sediments* (Ed. I.R. Kaplan), pp. 99–140. Plenum Press, New York.
- Compton, J.S.** (1988) Degree of supersaturation and precipitation of organogenic dolomite. *Geology*, **16**, 318–321.
- DeCarlo, E.H., Wen, X.-Y. and Irving, M.** (1998) The influence of redox reactions on the uptake of dissolved Ce by suspended Fe and Mn oxide particle. *Aquat. Geochem.*, **3**, 357–392.
- Decima, A. and Wezel, F.C.** (1971) Osservazioni sulle evaporiti messiniane della Sicilia centro-meridionale. *Riv. Miner. Siciliana*, **157–159**, 217–231.
- Decima, A. and Wezel, F.C.** (1973) Late Miocene evaporites of the central Sicilian basin, Italy. In: *Initial Reports of the Deep Sea Drilling Projects* (Eds W.B.F. Ryan, K.J. Hsü, M.B. Cita, P. Dumitrica, J.M. Lort, W. Mayne, W.D. Nesteroff, G. Pautot, H. Stradner and F.C. Wezel), Vol. 13, pp. 1234–1240. US Government Printing Office, Washington.

- Decima, A., McKenzie, J.A. and Schreiber, B.C. (1988) The origin of evaporative limestones: an example from the Messinian of Sicily (Italy). *J. Sed. Petrol.*, **58**, 256–272.
- Di Stefano, E., Cita, M.B., Spezzaferri, S. and Sprovieri, R. (1999) The Messinian-Zanclean Pissouri section (Cyprus, Eastern Mediterranean). *Mem. Soc. Geol. Ital.*, **54**, 133–144.
- Dupraz, C. and Visscher, P.T. (2005) Microbial lithification in marine stromatolites and hypersaline mats. *Trends Microbiol.*, **13**, 429–438.
- Dupraz, C., Visscher, P.T., Baumgartner, L.K. and Reid, R.P. (2004) Microbe-mineral interactions: early carbonate precipitation in a hypersaline lake (Eleuthera Island, Bahamas). *Sedimentology*, **51**, 745–765.
- Epstein, S., Graf, D.L. and Degens, E.T. (1964) Oxygen isotope studies on the origin of dolomite. In: *Isotopic and Cosmic Chemistry* (Eds H. Cray, S.L. Miller and G.T. Wassenburg), pp. 169–180. North-Holland, Amsterdam.
- Franzini, M., Leoni, L. and Saitta, M. (1975) Revisione di una metodologia analitica per fluorescenza X basata sulla correzione completa degli effetti di matrice. *Rend. Soc. Ital. Miner. Petrol.*, **21**, 99–108.
- Gabrielli, C., Maurin, G., Poindessous, G. and Rosset, R. (1999) Nucleation and growth of calcium carbonate by an electrochemical scaling process. *J. Cryst. Growth*, **200**, 236–250.
- Gaetani, G.A. and Cohen, A.L. (2006) Element partitioning during precipitation of aragonite from seawater: a framework for understanding paleoproxies. *Geochim. Cosmochim. Acta*, **70**, 4617–4634.
- Garcia-Pichel, F., Mechling, M. and Castenholz, R.W. (1994) Diel migrations of microorganisms within a benthic, hypersaline mat community. *Appl. Environ. Microbiol.*, **60**, 1500–1511.
- Gautier, F., Clauzon, G., Suc, J.P., Cravatte, J. and Violanti, D. (1994) Age et durée de la crise de salinité messinienne. *CR Acad. Sci. Paris*, **318**, 1103–1109.
- German, C.R. and Ederfield, H. (1990) Application of the Ce anomaly as a paleoredox indicator: the ground rule. *Paleoceanography*, **5**, 823–833.
- Goevert, D. and Conrad, R. (2008) Carbon isotope fractionation by sulphate-reducing bacteria using different pathways for the oxidation of acetate. *Environ. Sci. Technol.*, **42**, 7813–7817.
- Gromet, L.P., Dymek, R.F., Haskin, L.A. and Korotev, R.L. (1984) The 'North American shale composite': its compilation, major and trace element characteristics. *Geochim. Cosmochim. Acta*, **48**, 2469–2482.
- Guido, A., Jacob, J., Gautret, P., Laggoun-Défarge, F., Mastandrea, A. and Russo, F. (2007) Molecular fossils and other organic markers as palaeoenvironmental indicators of the Messinian Calcare di Base Formation: normal versus stressed marine deposition (Rossano Basin, northern Calabria, Italy). *Paleoceanogr. Palaeoclimatol. Palaeoecol.*, **255**, 265–283.
- Gundersen, J.K., Jørgensen, B.B., Larsen, E. and Jannasch, H.W. (1992) Mats of giant sulphur bacteria on deep-sea sediments due to fluctuating hydrothermal flow. *Nature*, **360**, 454–456.
- Herbert, R., Benner, S., Pratt, A. and Blowes, D. (1998) Surface chemistry and morphology of poorly crystalline iron sulfides precipitated in media containing sulfate-reducing bacteria. *Chem. Geol.*, **144**, 87–97.
- Hilgen, F.J. and Krijgsman, W. (1999) Cyclostratigraphy and astrochronology of the Tripoli diatomite formation (pre-evaporite Messinian, Sicily, Italy). *Terra Nova*, **11**, 16–22.
- Hilgen, F.G., Krijgsman, W., Langereis, C.G., Lourens, L.J., Santarelli, A. and Zachariasse, W.J. (1995) Extending the astronomical (polarity) time scale into the Miocene. *Earth Planet. Sci. Lett.*, **136**, 495–510.
- Hodell, D.A., Benson, R.H., Kent, D.V., Boersma, A. and Rakić-El Bied, K. (1994) Magnetostratigraphic, biostratigraphic, and stable isotope stratigraphy of an Upper Miocene drill core from the Salé Briqueterie (northwestern Morocco): a high-resolution chronology for the Messinian stage. *Paleoceanography*, **9**, 835–855.
- Holser, W.T. (1997) Evaluation of the application of rare-earth elements to paleoceanography. *Paleoceanogr. Palaeoclimat. Palaeoecol.*, **132**, 309–323.
- Hsü, K.J., Ryan, W.B.F. and Cita, M.B. (1973) Late Miocene desiccation of the Mediterranean. *Nature*, **242**, 240–244.
- Iversen, N. and Jørgensen, B.B. (1985) Anaerobic methane oxidation rates at the sulfate-methane transition in marine sediments from Kattegat and Skagerrak (Denmark). *Limnol. Oceanogr.*, **30**, 944–955.
- Jørgensen, C.K. (1970) The "tetrad effect" of Peppard is a variation of the nephelauxetic ratio in the third decimal. *J. Inorg. Nucl. Chem.*, **32**, 3127–3128.
- Jørgensen, B.B. and Cohen, Y. (1977) Solar Lake (Sinai): 5. The sulfur cycle of the benthic cyanobacterial mats. *Limnol. Oceanogr.*, **22**, 657–666.
- Jørgensen, B.B. and Revsbech, N.P. (1983) Colorless sulphur bacteria, *Beggiatoa* spp. and *Thiovolum* spp. in O₂ and H₂S microgradients. *Appl. Environ. Microbiol.*, **45**, 1261–1270.
- Kawabe, I. (1992) Lanthanide tetrad effect in the Ln³⁺ ionic radii and refined spin-pairing energy theory. *Geochem. J.*, **26**, 309–335.
- Kinsman, D.J.J. (1969) Interpretations of Sr²⁺ concentrations in carbonate minerals and rocks. *J. Sed. Petrol.*, **39**, 486–508.
- Krijgsman, W. and Zachariasse, W.J. (1994) The age of the Tortonian/Messinian boundary. *Earth Planet. Sci. Lett.*, **121**, 533–547.
- Krijgsman, W., Hilgen, F.J., Raffi, I., Sierro, F.J. and Wilson, D.S. (1999) Chronology, causes and progression of the Messinian Salinity Crisis. *Nature*, **400**, 652–655.
- Land, L.S. (1980) The isotopic and trace element geochemistry of dolomite: the state of the art. In: *Concepts and Models of Dolomitization* (Eds D.H. Zenger, J.B. Dunham and R.L. Ethington), *SEPM Spec. Publ.*, **28**, 87–110.
- Lyons, W.B., Long, D.T., Hines, M.E., Gaudette, H.E. and Armstrong, P.B. (1984) Calcification of cyanobacterial mats in Solar Lake, Sinai. *Geology*, **12**, 623–626.
- Machel, H.G. and Anderson, J.H. (1989) Pervasive subsurface dolomitization of the Nisku Formation in central Alberta. *J. Sed. Petrol.*, **59**, 891–911.
- Manzi, V., Lugli, S. and Roveri, M. (2007) New insights on the Messinian Upper Evaporites of Sicily (Italy). *Geotitalia*, Epitome, **2**, 393. Rimini, 12–14 September 2007.
- Martín, J.M. and Braga, J.C. (1994) Messinian events in the Sorbas basin in southeastern Spain and their implications in the recent history of the Mediterranean. *Sed. Geol.*, **90**, 257–268.
- Masuda, A. and Ikeuchi, Y. (1979) Lanthanide tetrad effect observed in marine environment. *Geochem. J.*, **13**, 19–22.
- Masuda, A., Kawakami, O., Dohmoto, Y. and Takenaka, T. (1987) Lanthanide tetrad effects in nature: two mutually opposite types, W and M. *Geochem. J.*, **21**, 119–124.
- McKenzie, J.A. (1981) Holocene dolomitization of calcium carbonate sediments from the coastal sabkhas of Abu Dhabi, UAE: a stable isotope study. *J. Geol.*, **89**, 185–198.
- McKenzie, J.A. (1985) Stable isotope mapping in Messinian evaporative carbonates of central Sicily. *Geology*, **13**, 851–854.

- McKenzie, J.A., Jenkyns, H.C. and Bennet, G.G.** (1979–1980) Stable isotope study of the cyclic diatomite-claystones from the Tripoli formation, Sicily: a prelude to the Messinian salinity crisis. *Palaeogeogr. Palaeoclimatol. Palaeoecol.*, **29**, 125–142.
- McLennan, S.M.** (1989) Rare earth elements in sedimentary rocks: influence of provenance and sedimentary processes. In: *Geochemistry and Mineralogy of Rare Earth Elements* (Eds B.R. Lipin and G.A. McKay), pp. 169–200. Mineralogical Society of America, Washington.
- Megonigal, J.P., Hines, M.E. and Visscher, P.T.** (2003) Anaerobic metabolism: linkages to trace gases and aerobic processes. In: *Treatise on Geochemistry* (Ed. W.H. Schlesinger), Vol. **8**, pp. 317–424. Elsevier, Amsterdam.
- Meister, P., McKenzie, J.A., Vasconcelos, C., Bernasconi, S., Frank, M., Gutjahr, M. and Schrag, D.P.** (2007) Dolomite formation in the dynamic deep biosphere: results from the Peru Margin. *Sedimentology*, **54**, 1007–1032.
- Middleburg, J.J., Lange, G.J.D. and Kreulen, R.** (1990) Dolomite formation in anoxic sediments of Kau Bay, Indonesia. *Geology*, **18**, 399–402.
- Miller, N.R. and Leybourne, M.I.** (2003) Reconstructing basin bottom-water evolution from microbial time capsules: rare earth element geochemistry of organogenic dolomite in the Miocene Monterey Formation. *Seattle Annual Meeting*. Paper No. 256-5 2–5 November 2004, Washington..
- Moffett, J.W.** (1990) Microbially mediated cerium oxidation in sea water. *Nature*, **345**, 421–423.
- Moffett, J.W.** (1994) The relationship between cerium and manganese oxidization in the marine environment. *Limnol. Oceanogr.*, **39**, 1309–1318.
- Møller, M.M., Nielsen, L.P. and Jørgensen, B.B.** (1985) Oxygen responses and mat formation by *Beggiatoa* spp. *Appl. Environ. Microbiol.*, **50**, 373–382.
- Monty, C.L.V.** (1965) Distribution and structure of recent stromatolitic algal mats, Eastern Andros Island, Bahamas. *Ann. Soc. Geol. Belg.*, **96**, 265–267.
- Müller, D.W. and Hsü, K.J.** (1987) Event stratigraphy and paleoceanography in the Fortuna basin (southeast Spain): a scenario for the Messinian salinity crisis. *Paleoceanography*, **6**, 679–696.
- Murata, K.J., Friedman, I. and Madsen, B.M.** (1969) Isotopic composition of diagenetic carbonates in Miocene marine formations in California and Oregon. *US Geol. Surv.*, Professional Paper, **724-C**, 12 pp.
- Murray, R.W., Buccholtz ten Brink, M.R., Gerlach, D.C., Russ III, G.P. and Jones, D.L.** (1991) Rare earth, major, and trace elements in chert from the Franciscan Complex and Monterey Group, California: assessing REE source to fine-grained marine sediments. *Geochim. Cosmochim. Acta*, **55**, 1875–1895.
- Nealson, K.H.** (1997) Sediment bacteria: who's there, what they are doing, and what's new. *Annu. Rev. Earth Planet. Sci.*, **51**, 403–434.
- Nothdurft, L.D., Webb, G.E. and Kamber, B.S.** (2004) Rare earth element geochemistry of Late Devonian reefal carbonates, Canning Basin, Western Australia: confirmation of a seawater REE proxy in ancient limestones. *Geochim. Cosmochim. Acta*, **68**, 263–283.
- Nugent, L.J.** (1970) Theory of the tetrad effect in the lanthanide(III) and actinide(III) series. *J. Inorg. Nucl. Chem.*, **32**, 3485–3491.
- Ogniben, L.** (1957) Petrografia della Serie Solifera Siciliana e considerazioni geologiche relative. *Mem. Descr. Carta Geol. Ital.*, **33**, 275 pp.
- Ogniben, L.** (1963) Sedimenti halitico-calcitici a struttura grumosa nel Calcare di Base Messiniano in Sicilia. *Giorn. Geol.*, **31**, 509–542.
- Olivier, N. and Boyet, M.** (2006) Rare earth and trace elements of microbialites in Upper Jurassic coral- and sponge-microbialite reefs. *Chem. Geol.*, **230**, 105–123.
- Orcutt, B., Boetius, A., Elvert, M., Samarkin, V. and Joye, S.B.** (2005) Molecular biogeochemistry of sulfate reduction, methanogenesis and the anaerobic oxidation of methane at Gulf of Mexico cold seeps. *Geochim. Cosmochim. Acta*, **69**, 4267–4281.
- Peckmann, J., Thiel, V., Reitner, J., Taviani, M., Aharon, P. and Michaelis, W.** (2004) A microbial mat of a large sulfur bacterium preserved in a Miocene methane-seep limestone. *Geomicrobiol. J.*, **21**, 247–255.
- Peppard, D.F., Mason, G.W. and Lewey, S.** (1969) A tetrad effect in the liquid-liquid extraction ordering of lanthanide(III). *J. Inorg. Nucl. Chem.*, **31**, 2271–2272.
- Pierre, C. and Rouchy, J.M.** (1990) Sedimentary and diagenetic evolution of Messinian evaporites in the Thyrrenian Sea (ODP Leg 107, Sites 652, 653 and 654): petrographic, mineralogical, and stable isotope records. In: *Proc. ODP Sc. Results* (Eds K.A. Kastens, J. Mascle *et al.*), Vol. **107**, pp. 187–210, Ocean Drilling Program, College Station, TX.
- Piper, D.Z.** (1974) Rare earth elements in the sedimentary cycle: a summary. *Chem. Geol.*, **14**, 285–304.
- Reeburgh, W.S.** (1976) Methane consumption in Cariaco Trench waters and sediments. *Earth Planet. Sci. Lett.*, **28**, 337–344.
- Reid, R.P., Visscher, P.T., Decho, A.W., Stolz, J.F., Bebout, B.M., Dupraz, C., Macintyre, I.G., Paerl, H.W., Pinckney, J.L., Prufert-Bebout, L., Steppe, T.F. and Des Marais, D.J.** (2000) The role of microbes in accretion, lamination and early lithification of modern marine stromatolites. *Nature*, **406**, 989–992.
- Riding, R.** (2000) Microbial carbonates: the geological record of calcified bacterial-algal mats and biofilms. *Sedimentology*, **47**(Suppl. 1), 179–214.
- Riding, R. and Awramik, S.M.** (2000) *Microbial Sediments*. Springer, Berlin, 331 pp.
- Riding, R. and Tomás, S.** (2006) Stromatolite reef crusts, Early Cretaceous, Spain: bacterial origin of *in situ*-precipitated peloid microspar? *Sedimentology*, **53**, 23–34.
- Riding, R., Braga, J.C., Martín, J.M. and Sanchez-Almazo, I.M.** (1998) Mediterranean Messinian Salinity Crisis: constraints from a coeval marginal basin, Sorbas, southeastern Spain. *Mar. Geol.*, **146**, 1–20.
- Riding, R., Braga, J.C. and Martín, J.M.** (2000) Late Miocene Mediterranean dessication: topography and significance of the “Salinity Crisis” erosion surface on-land in southeast Spain. *Sed. Geol.*, **133**, 175–184.
- Rosen, M.R., Miser, D.E., Starcher, M.A. and Warren, J.K.** (1989) Formation of dolomite in the Coorong region, South Australia. *Geochim. Cosmochim. Acta*, **53**, 661–669.
- Rouchy, J.M.** (1982) La genèse des évaporites messiniennes de Méditerranée. *Mem. Mus. Nat. Hist. Nat.*, **L**, 267 pp.
- Rouchy, J.M.** (1986) Sédimentologie des formations anhydritiques givétiennes et dinantiennes du segment varisque franco-belge. *Bull. Soc. belge géol.*, **95**, 111–128.
- Rouchy, J.M. and Caruso, A.** (2006) The Messinian salinity crisis in the Mediterranean basin: a reassessment of the data and an integrated scenario. *Sed. Geol.*, **188–189**, 35–67.
- Rouchy, J.M. and Monty, C.L.V.** (1981) Stromatolites and cryptalgal laminites associated with Messinian gypsum of

- Cyprus. In: *Phanerozoic Stromatolites* (Ed. C.L.V. Monty), pp. 155–178. Springer, Berlin.
- Rouchy, J.M. and Saint-Martin, J.P.** (1992) Late Miocene events in the Mediterranean as recorded by carbonate-evaporite relations. *Geology*, **20**, 629–632.
- Rouchy, J.M., Taberner, C., Blanc-Valleron, M.M., Sprovieri, R., Russel, M., Pierre, C., Di Stefano, E., Pueyo, J.J., Caruso, A., Dinares-Turrel, J., Gomis-Coll, E., Cespuglio, G., Ditchfield, P., Grimalt, J., Pestrea, S., Combourieu-Nebout, N. and Santisteban, C.** (1998) Sedimentary and diagenetic markers of the restriction in a marine basin: the Lorca (SE Spain) during the Messinian. *Sed. Geol.*, **121**, 23–55.
- Rouchy, J.M., Orszag-Sperber, F., Blanc-Valleron, M.M., Pierre, C., Rivière, M., Combourieu-Nebout, N. and Panaydes, I.** (2001) Paleoenvironmental changes at the Messinian-Pliocene boundary in the eastern Mediterranean: southern Cyprus basins. *Sed. Geol.*, **145**, 93–117.
- Roveri, M., Bassetti, M.A. and Ricci Lucchi, F.** (2001) The Mediterranean Messinian salinity crisis: an Apennine fore-deep perspective. *Sed. Geol.*, **140**, 201–214.
- Roveri, M., Lugli, S., Manzi, V. and Schreiber, B.C.** (2008) The Messinian Sicilian stratigraphy revisited: new insights for the Messinian salinity crisis. *Terra Nova*, **20**, 483–488.
- Schmidt, M., Xeflide, S., Botz, R. and Mann, S.** (2005) Oxygen isotope fractionation during synthesis of Ca-Mg-carbonate and implications for sedimentary dolomite formation. *Geochim. Cosmochim. Acta*, **69**, 4665–4674.
- Schultz, L.G.** (1964) Quantitative interpretations of mineralogic composition from X-ray and chemical data for the Pierre Shale. *US Geol. Surv. Prof. Pap.* 391-C, C1–C31.
- Shields, G. and Webb, G.E.** (2004) Has the REE composition of seawater changed over geological time? *Chem. Geol.*, **204**, 103–107.
- Sholkovitz, E.R.** (1988) Rare earth elements in the sediments of the North Atlantic Ocean, Amazon Delta, and East China Sea: reinterpretation of terrigenous input patterns to the oceans. *Am. J. Sci.*, **288**, 236–281.
- Sholkovitz, E.R. and Schneider, D.L.** (1991) Cerium redox cycles and rare earth elements in the Sargasso Sea. *Geochim. Cosmochim. Acta*, **55**, 2737–2743.
- Sprachta, S., Camoin, G., Golubic, S. and Le Campion, Th.** (2001) Microbialites in a modern lagoonal environment: nature and distribution, Tikehau atoll (French Polynesia). *Palaeogeogr. Palaeoclimatol. Palaeoecol.*, **175**, 103–124.
- Suc, J.P., Violante, D., Londeix, L., Poumot, C., Robert, C., Clauzon, G., Gautier, F., Turon, J.-L., Ferrier, J., Chikhi, H. and Cambon, G.** (1995) Evolution of the Messinian Mediterranean environments: the Tripoli Formation at Capodarso (Sicily, Italy). *Rev. Palaeobot. Palynol.*, **87**, 51–79.
- Takahashi, Y., Châtellier, X., Hattori, K.H., Kato, K. and Fortin, D.** (2005) Adsorption of rare earth elements onto bacterial cell walls and its implication for REE sorption onto natural microbial mats. *Chem. Geol.*, **219**, 53–67.
- Takahashi, Y., Hirata, T., Shimizu, H., Ozaki, T. and Fortin, D.** (2007) A rare earth element signature of bacteria in natural waters? *Chem. Geol.*, **244**, 569–583.
- Tamajo, E.** (1961) Probabili tracce di vita in livelli ritenuti azoici della formazione zolfifera siciliana. *Riv. Min. Siciliana*, **67**, 6–14.
- Thomson, J., Crudeli, D., De Lange, G.J., Slomp, C., Erba, E. and Corselli, C.** (2004) Florisphaera profunda and the origin and diagenesis of carbonate phases in eastern Mediterranean sapropel units. *Paleoceanography*, **19**, PA3003; doi: 10.1029/2003PA000976.
- Tlig, S. and M'Rabet, A.** (1985) A comparative study of the rare earth element (REE) distributions within the Lower Cretaceous dolomites and limestones of Central Tunisia. *Sedimentology*, **32**, 897–907.
- Tucker, M.E.** (2001) *Sedimentary Petrology*. Blackwell Scientific Publications, Oxford, 262 pp.
- Vai, G.B. and Ricci Lucchi, F.** (1977) Algal crust, authochthonous and clastic gypsum in a cannibalistic evaporite basin: a case history from Messinian of Northern Apennines. *Sedimentology*, **24**, 211–244.
- Van der Zwaan, G.J.** (1979) The pre-evaporite late Miocene environment of the Mediterranean; stable isotopes of planktonic foraminifera from section Falconara, Sicily. *Kon. Ned. Akad. Wetens., Proc.*, **82**, 487–502.
- Van Lith, Y., Warthmann, R., Vasconcelos, C. and McKenzie, J.A.** (2003) Sulphate-reducing bacteria induce low-temperature Ca-dolomite and high Mg-calcite formation. *Geobiology*, **1**, 71–79.
- Vasconcelos, C. and McKenzie, J.A.** (1997) Microbial mediation of modern dolomite precipitation and diagenesis under anoxic condition (Lagoa Vermelha, Rio de Janeiro, Brazil). *J. Sed. Res.*, **67**, 378–390.
- Vasconcelos, C., McKenzie, J.A., Bernasconi, S., Grujic, D. and Tien, A.J.** (1995) Microbial mediation as a possible mechanism for natural dolomite formation at low temperatures. *Nature*, **377**, 220–222.
- Visscher, P.T., Reid, R.P., Bebout, B.M., Hoefft, S.E., Macintyre, I.G. and Thompson, J.A.** (1998) Formation of lithified micritic laminae in modern marine stromatolites (Bahamas): the role of sulfur cycling. *Am. Mineral.*, **83**, 1482–1493.
- Visscher, P.T., Reid, R.P. and Bebout, B.M.** (2000) Microscale observations of sulphate reduction: correlation of microbial activity with lithified micritic laminae in modern marine stromatolites. *Geology*, **28**, 919–922.
- Walter, L.M., Bischof, S.A., Patterson, W.P., Lyons, T.W., O'Nions, R.K., Gruszczynski, M., Sellwood, B.W. and Coleman, M.L.** (1993) Dissolution and recrystallization in modern shelf carbonates: evidence from pore water and solid phase chemistry. *Phil. Trans. Roy. Soc. London A*, **344**, 27–36.
- Warthmann, R., van Lith, Y., Vasconcelos, C., McKenzie, J.A. and Karpoff, A.M.** (2000) Bacterially induced dolomite precipitation in anoxic culture experiments. *Geology*, **28**, 1091–1094.
- Webb, G.E. and Kamber, B.S.** (2000) Rare earth elements in Holocene reefal microbialites: a new shallow seawater proxy. *Geochim. Cosmochim. Acta*, **64**, 1557–1565.
- Whiticar, M.J., Faber, E. and Schoell, M.** (1986) Biogenic methane formation in marine and freshwater environments: CO₂ reduction vs. acetate fermentation: isotope evidence. *Geochim. Cosmochim. Acta*, **50**, 693–709.
- Wright, D.T.** (1999) The role of sulphate-reducing bacteria and cyanobacteria in dolomite formation in distal ephemeral lakes of the Coorong region, South Australia. *Sed. Geol.*, **126**, 147–157.
- Wright, D.T. and Wacey, D.** (2005) Precipitation of dolomite using sulphate-reducing bacteria from the Coorong Region, South Australia: significance and implication. *Sedimentology*, **52**, 987–1008.

Manuscript received 7 October 2008; revision accepted 21 July 2009